THE JOURNAL OF IMMUNOLOGY

Development of Mature and Functional Human Myeloid Subsets in Hematopoietic Stem Cell-Engrafted NOD/SCID/IL2rγKO Mice

Satoshi Tanaka, Yoriko Saito, Jun Kunisawa, Yosuke Kurashima, Taichi Wake, Nahoko Suzuki, Leonard D. Shultz, Hiroshi Kiyono and Fumihiko Ishikawa

J Immunol 2012; 188:6145-6155; Prepublished online 18 May 2012;
doi: 10.4049/jimmunol.1103660
http://www.jimmunol.org/content/188/12/6145

The Journal of Immunology is published twice each month by The American Association of Immunologists, Inc., 9650 Rockville Pike, Bethesda, MD 20814-3994.

Print ISSN: 0022-1767 Online ISSN: 1550-6606.

Development of Mature and Functional Human Myeloid Subsets in Hematopoietic Stem Cell-Engrafted NOD/SCID/IL2rγKO Mice

Satoshi Tanaka,*,†,‡,§ Yoriko Saito,‡ Jun Kunisawa,*,† Yosuke Kurashima,† Taichi Wake,† Nahoko Suzuki,‡ Leonard D. Shultz,¶ Hiroshi Kiyono,*,†,‖ and Fumihiko Ishikawa‡

Although physiological development of human lymphoid subsets has become well documented in humanized mice, in vivo development of human myeloid subsets in a xenotransplantation setting has remained unevaluated. Therefore, we investigated in vivo differentiation and function of human myeloid subsets in NOD/SCID/IL2rγ^{null} (NSG) mouse recipients transplanted with purified lineage$^-$CD34$^+$CD38$^-$ cord blood hematopoietic stem cells. At 4–6 mo posttransplantation, we identified the development of human neutrophils, basophils, mast cells, monocytes, and conventional and plasmacytoid dendritic cells in the recipient hematopoietic organs. The tissue distribution and morphology of these human myeloid cells were similar to those identified in humans. After cytokine stimulation in vitro, phosphorylation of STAT molecules was observed in neutrophils and monocytes. In vivo administration of human G-CSF resulted in the recruitment of human myeloid cells into the recipient circulation. Flow cytometry and confocal imaging demonstrated that human bone marrow monocytes and alveolar macrophages in the recipients displayed intact phagocytic function. Human bone marrow-derived monocytes/macrophages were further confirmed to exhibit phagocytosis and killing of *Salmonella typhimurium* upon IFN-γ stimulation. These findings demonstrate the development of mature and functionally intact human myeloid subsets in vivo in the NSG recipients. In vivo human myelopoiesis established in the NSG humanized mouse system may facilitate the investigation of human myeloid cell biology including in vivo analyses of infectious diseases and therapeutic interventions. *The Journal of Immunology*, **2012, 188: 6145–6155.**

The use of genetically modified mice has led to significant advances in biomedical research by providing insights into the role of individual genes both in normal physiology and in disease pathogenesis. However, translation of these findings into effective therapies for human diseases has been limited by the gap that exists between murine and human biology. The availability of human samples (e.g., cells and tissues), although supporting successful translation from bench research to clinical medicine, is limited by both logistic and ethical concerns.

Therefore, mice repopulated with human hematopoietic cells through xenogeneic transplantation were developed directly to investigate the human immuno-hematopoietic system in vivo. Based on pioneering work using the Hu-PBL-SCID (1) and SCID-hu (2) systems, investigators have aimed to improve xenotransplantation models using immunodeficient strains of mice as recipients of human hematopoietic stem cells (HSCs) to achieve long-term engraftment of multiple human hematopoietic and immune subsets (3). NOD/SCID mice, established by back-crossing the *scid* mutation onto the NOD strain background, are characterized by partially impaired innate immunity and deficient complement-dependent cytotoxicity and are the gold standard for stable human hematopoietic stem/progenitor cell engraftment (3, 4). The ability of NOD-*scid* mice to support human HSC engraftment is associated with a human-like polymorphism in the IgV domain of the signal regulatory protein-α (*Sirpa*) allele in the NOD strain background resulting in the expression of SIRPα with enhanced binding of human CD47 (5). The interaction between SIRPα and CD47 has previously been implicated in the negative regulation of phagocytosis by macrophages through a "do-not-eat-me signal" (6).

The introduction of IL2r common γ-chain mutations onto the NOD/SCID and BALBc/Rag2KO backgrounds led to the generation of the NOD/SCID/γ_c^{null} (NOG) (7, 8) strain with a truncated IL-2Rγ, the NOD/SCID/IL2rγ^{null} (NSG) (9, 10) strain with a complete IL-2Rγ-null mutation, and BALB/c-Rag2KO/γ_c^{null} mice (11), resulting in more profound defects in innate immunity. In vivo human hematopoietic repopulation through transplantation

*Department of Medical Genome Sciences, Graduate School of Frontier Sciences, The University of Tokyo, Chiba, Japan; †Division of Mucosal Immunology, The Institute of Medical Science, The University of Tokyo, Tokyo, Japan; ‡Research Unit for Human Disease Models, RIKEN Research Center for Allergy and Immunology, Yokohama, Japan; §Nippon Becton Dickinson Company, Tokyo, Japan; ¶The Jackson Laboratory, Bar Harbor, ME; and ‖Core Research for Evolutional Science and Technology, Japan Science and Technology Agency, Tokyo, Japan

Received for publication December 30, 2011. Accepted for publication April 19, 2012.

This work was supported by grants from the Ministry of Education, Culture, Sports, Science and Technology of Japan and from the Takeda Science Foundation (to F.I.); grants from the Ministry of Education, Culture, Sports, Science and Technology of Japan (to H.K. and J.K.); the Program for Promotion of Basic and Applied Researches for Innovations in Bio-oriented Industry (to J.K.); and grants from the National Institutes of Health, the U.S. Army Medical Research Institute of Infectious Diseases, and the Helmsley Foundation (to L.D.S.). Y.K. is a Japan Society for the Promotion of Science fellow.

Address correspondence and reprint requests to Fumihiko Ishikawa, Research Unit for Human Disease Models, RIKEN Research Center for Allergy and Immunology, 1-7-22 Suehiro-cho Tsurumi-ku, Yokohama 230-0045, Japan. E-mail address: f_ishika@rcai.riken.jp

The online version of this article contains supplemental material.

Abbreviations used in this article: BM, bone marrow; CB, cord blood; cDC, conventional dendritic cell; DC, dendritic cell; HSC, hematopoietic stem cell; MNC, mononuclear cell; MOI, multiplicity of infection; PB, peripheral blood; pDC, plasmacytoid dendritic cell; rhG-CSF, recombinant human G-CSF; rhGM-CSF, recombinant human GM-CSF; rhIFN-γ, recombinant human IFN-γ; rhM-CSF, recombinant human M-CSF.

www.jimmunol.org/cgi/doi/10.4049/jimmunol.1103660

of human $CD34^+$ or $CD34^+CD38^-$ HSCs in these severely immunocompromised recipients accelerated human stem cell and immunology research by allowing higher levels of human HSC engraftment, differentiation of human T cells in the murine thymus and secondary lymphoid organs, enhanced maturation of human B cells, and human immune function in vivo (7–12).

Despite these advances, one of the remaining issues to be clarified in humanized mouse research has been the development of human myeloid lineage cells in the host mouse tissues. To date, we and others reported the development of human $CD33^+$ myeloid cells and myeloid subsets in NOG mice, BALB/c-Rag2KO/γ_c^{null} mice, and NSG mice (7, 9, 11, 13). In this study, by using NSG newborns as recipients, we present in vivo differentiation of human myeloid subsets in the bone marrow (BM), spleen, and respiratory tract of NSG mice engrafted with purified lineage$^-CD34^+CD38^-$ human cord blood (CB) HSCs. Human granulocytes (neutrophils, basophils, and mast cells) and APCs (monocytes/macrophages, conventional dendritic cells [cDCs] and plasmacytoid dendritic cells [pDCs]) developing in NSG mice exhibited characteristics of human myeloid cells including morphological features and expression of surface molecules known to be associated with the myeloid cell subsets. Moreover, human myeloid cells developing in the NSG recipients displayed functionality such as responsiveness to cytokine or TLR adjuvant and phagocytic function. The in vivo system supporting the development of mature human myeloid cells with intact function will facilitate the evaluation of human myeloid development from hematopoietic stem/progenitor cells, advance in vivo investigation of human myeloid cell-mediated immune responses against pathogens and malignancies, and will support studies of therapeutic agents.

Materials and Methods

Mice

NOD.Cg-*Prkdc*^{scid}*IL2rg*^{tm1Wjl}/Sz (NSG) mice were developed at The Jackson Laboratory by back-crossing a complete null mutation at the *Il2rg* locus onto the NOD.Cg-*Prkdc*^{scid} (NOD/SCID) strain (9, 10). Mice were bred and maintained under defined flora with irradiated food at the animal facility of RIKEN and at The Jackson Laboratory according to guidelines established by the institutional animal committees at each respective institution.

Purification of human HSCs and xenogeneic transplantation

All experiments were performed with authorization from the Institutional Review Board for Human Research at RIKEN Research Center for Allergy and Immunology. CB samples were first separated for mononuclear cells (MNCs) by LSM lymphocyte separation medium (MP Biomedicals). CB MNCs were then enriched for human $CD34^+$ cells by using anti-human CD34 microbeads (Miltenyi Biotec) and sorted for 7AAD$^-$lineage(hCD3/hCD4/hCD8/hCD19/hCD56)$^-CD34^+CD38^-$ HSCs using FACSAria (BD Biosciences). To achieve high purity of donor HSCs, doublets were excluded by analysis of forward scatter-height/forward scatter-width and side scatter-height/side scatter-width. The purity of HSCs was higher than 98% after sorting. Newborn (within 2 d of birth) recipients received 150 cGy total body irradiation using a ^{137}Cs-source irradiator, followed by i.v. injection of 1×10^4–3×10^4 sorted HSCs via the facial vein (14). The recipient peripheral blood (PB) harvested from the retro-orbital plexus was evaluated for human hematopoietic engraftment every 3 to 4 wk starting at 6 wk posttransplantation. At 4–6 mo posttransplantation, recipient mice were euthanized for analysis.

Flow cytometry

Erythrocytes in the PB were lysed with Pharm Lyse (BD Biosciences). Single-cell suspensions were prepared from BM and spleen using standard procedures. To isolate MNCs from the lung, lung tissues were carefully excised, teased apart, and dissociated using collagenase (Wako) (15). The following mAbs were used for identifying engraftment of human hematopoietic cells in NSG recipients: anti-human CD3 V450 (clone UCHT1) and PE–Cy5 (HIT3a), anti-hCD4 PE–Cy5 (RPA-T4), anti-hCD8 PE–Cy5 (RPA-T8), anti-hCD11b/Mac-1 Pacific blue (ICRF44), anti-hCD11c allophycocyanin (B-ly6), anti-hCD14 Alexa700 (M5E2), allophycocyanin–H7 and V450 (MϕP9), anti-hCD15 allophycocyanin (HI98) and V450 (MMA), anti-hCD19 PerCP–Cy5.5, PE–Cy5 and PE–Cy7 (SJ25C1), anti-hCD33 PE and PE–Cy7 (p67.6), anti-hCD34 PE–Cy7 (8G12), anti-hCD38 FITC and allophycocyanin (HB7), anti-hCD45, V450 and V500 (HI30), anti-hCD45 AmCyan and allophycocyanin–Cy7 (2D1), anti-hCD56 FITC (NCAM16.2) and PE–Cy5 (B159), anti-hCD114/G-CSFR PE (LMM741), anti-hCD116/GM-CSFR FITC (hGMCSFR-M1), anti-hCD117/c-Kit PerCP–Cy5.5 (104D2), anti-hCD119/IFN-γR PE (GIR-208), anti-hCD123/IL-3R PE and PerCP–Cy5.5 (7G3), anti-hCD284/TLR2 Alexa647 (11G7), anti–HLA-DR allophycocyanin–H7 (L243), anti-mouse CD45 PerCP–Cy5.5 and allophycocyanin–Cy7 (30-F11), all from BD Biosciences; anti-human CD1c/BDCA-1 FITC (AD5-8E7), anti-hCD141/BDCA-3 FITC, PE and allophycocyanin (AD5-14H12), anti-hCD303/BDCA-2 PE (AC144) from Miltenyi; anti-human CD115/M-CSFR PE (9-4D2-1E4), anti-hCD203c/E-NPP3 PE (NP4D6), anti-hCD284/TLR4 PE (HTA125), anti-hFcεRI FITC (AER-37), anti-mouse CD45 Alexa700 (30-F11) from BioLegend. The labeled cells were analyzed using FACSCantoII or FACSAria (BD Biosciences).

Morphological analysis

Cytospin specimens of FACS-purified human myeloid cells were prepared with a Shandon Cytospin 4 cytocentrifuge (Thermo Electric). To identify nuclear and cytoplasmic characteristics of each myeloid cell, cytospin specimens were stained with 100% May–Grünwald solution (Merck) for 3 min, followed by 50% May–Grünwald solution in phosphate buffer (Merck) for an additional 5 min, and then with 5% Giemsa solution (Merck) in phosphate buffer for 15 min. All staining procedures were performed at room temperature. Light microscopy was performed with a Zeiss Axiovert 200 (Carl Zeiss).

In vitro cytokine stimulation and phospho-specific flow cytometry

After 2-h preculture at 37°C in RPMI 1640 (Sigma) containing 10% FBS, recipient BM cells were incubated for 15 min in medium supplemented with 100 ng/ml recombinant human IFN-γ (rhIFN-γ; BD Biosciences), 100 ng/ml recombinant human G-CSF (rhG-CSF; PeproTech), 100 ng/ml recombinant human GM-CSF (rhGM-CSF; PeproTech) or 100 ng/ml recombinant human M-CSF (rhM-CSF; R&D Systems), fixed for 10 min at 37°C with Phosflow Lyse/Fix Buffer (BD Biosciences), permeabilized for 15 min at 4°C with 0.5× Phosflow Perm Buffer IV (BD Biosciences), and labeled using the following set of Abs: anti-human CD3 PerCP–Cy5.5 (SK7), anti-hCD14 PE (M5E2), anti-hCD15 allophycocyanin (HI98), anti-hCD33 PE–Cy7 (p67.6), anti-hCD45 V450 (HI30), anti-mouse CD45 allophycocyanin–Cy7 (30-F11), and the combination of anti-human p-STAT1 Alexa488 (4a), p-STAT3 Alexa488 (4/P-STAT3), p-STAT4 Alexa488 (38/p-Stat4), p-STAT5 Alexa488, and p-STAT6 Alexa488 (18/P-Stat6), all from BD Biosciences. Phosphorylation of STAT molecules was analyzed using FACSCantoII (BD Biosciences). Digital data were converted into a heat map using an online analysis system (Cytobank; http://www.cytobank.org/) (16).

In vivo rhG-CSF treatment of humanized NSG mice

Human CB HSC-engrafted NSG recipients at 4–6 mo posttransplantation were given rhG-CSF (PeproTech) at 300 μg/kg s.c. once a day for five consecutive days. The recipients were analyzed for the frequency of $hCD45^+CD15^+CD33^{low}$ fraction (neutrophils) and $hCD45^+CD15^{-/low}$ $CD33^+$ fraction (monocytes and DCs) before and after rhG-CSF treatment.

In vitro phagocytosis by human myeloid subsets

In vitro phagocytosis was examined using Fluoresbrite Yellow Green carboxylate microspheres (Polysciences). After single-cell preparation, recipient lung and BM cells were precultured for 2 h at 37°C in RPMI 1640 (Sigma) containing 10% FBS then incubated with fluorescent beads (particle/cell ratio = 10:1) for 1 h at 37°C or 4°C and labeled with anti-mouse CD45 allophycocyanin–Cy7, anti-human CD45 allophycocyanin and anti-hCD33 PE–Cy7 (all from BD Biosciences) for identification of fluorescent beads$^+$ $hCD45^+hCD33^+$ cells. The frequencies of observed fluorescent beads$^+$ $hCD45^+hCD33^+$ cells out of total $hCD45^+hCD33^+$ cells were determined. Fluorescent beads$^+$ $hCD45^+hCD33^+$ human lung myeloid cells were purified using FACSAria (BD Biosciences) and imaged using a laser-scanning confocal microscope (Zeiss LSM 710; Carl Zeiss). The intracellular localization of fluorescent beads was confirmed by scanning z-series sections.

TLR analysis and in vivo LPS stimulation of humanized NSG mice

Surface expression levels of TLR2 and TLR4 were analyzed by FACSCantoII. To test the LPS-induced inflammatory response, human CB

HSC-engrafted NSG recipients at 4–6 mo posttransplantation were injected i.v. with LPS at 15 μg/mouse. After LPS injection, plasma was collected from 0 to 4 h. Human cytokines IL-1β, IL-6, IL-8, IL-10, IL-12p70, and TNF were measured by cytometric bead array (BD Biosciences).

IFN-γ–induced Salmonella *killing activity by humanized mouse-derived monocytes/macrophages*

Salmonella typhimurium PhoPc strain transformed with the pKKGFP plasmid was kindly provided by J.P. Kraehenbuhl (17). *S. typhimurium* was grown shaking at 180 rpm overnight in Luria–Bertani broth supplemented with 100 μg/ml ampicillin at 37°C. BM monocytes/macrophages were purified by FACSAria (BD) based on the phenotypic characterization of lineage (CD3, CD7, CD16, CD19, CD56, CD123, CD235a)-negative, mouse CD45 and Ter119-negative, human $CD45^+CD11b^+$. Aliquots of (10^4) human monocytes/macrophages derived from humanized mouse BM were cultured on collagen type I-coated 96-well plates (BD) for 24 h in either the presence or the absence of 1000 U/ml recombinant human IFN-γ (BD). Then, cells were infected with *S. typhimurium* at multiplicity of infection (MOI) of 20 at 37°C for 2 h, and the infection was confirmed by fluorescence microscopy (Biorevo BZ-9000; Keyence). For intracellular CFU determination, cells were washed twice with PBS and lysed in 0.2% Triton X-100 in PBS for 2 min, and lysates were diluted and plated onto Luria–Bertani broth agar plates containing 100 μg/ml ampicillin for colony enumeration.

Statistical analysis

The numerical data are presented as means ± SEM unless otherwise noted. Where noted, two-tailed *t* tests were performed, and the differences with the *p* value <0.05 were deemed statistically significant (GraphPad Prism; GraphPad).

Results

Human myeloid lineage cells develop in NSG mice transplanted with human CB HSCs

Recent advances in our knowledge of innate immunity reemphasize the importance of myeloid cells for sensing, capturing, and processing Ags for the initiation of innate and acquired phases of immune responses. The development of human myeloid cells in HSC-engrafted NSG mice has not previously been studied in detail. To evaluate in vivo differentiation and function of human myeloid lineage cell populations, we transplanted 1×10^4–3×10^4 purified human $lineage^-CD34^+CD38^-$ CB HSCs intravenously into sublethally irradiated newborn NSG mice. At 4–6 mo posttransplantation, we confirmed high levels of human hematopoietic chimerism and multilineage differentiation of human immune subsets as evidenced by flow cytometry (Fig. 1A, 1B). In addition to the reconstitution of human adaptive immunity ($CD3^+$ T cells and $CD19^+$ B cells), we identified the development of human innate immune cell subsets such as $CD56^+$ NK cells and $CD33^+$ myeloid cells in the recipient mice. The frequency of human myeloid lineage cells was higher in the recipient BM (30.7 ± 3.9%, $n = 11$) compared with that in the spleen (6.2 ± 1.2%, $n = 11$, $p < 0.0001$ by paired two-tailed *t* test) and PB (7.1 ± 1.3%, $n = 11$, $p < 0.0003$) (Fig. 1B).

We then identified the subsets of human myeloid cells present in the humanized NSG recipient mice through flow cytometry. Human myeloid subsets are classified into HLA class II-negative granulocytes and class II-positive APCs. In the BM and spleen

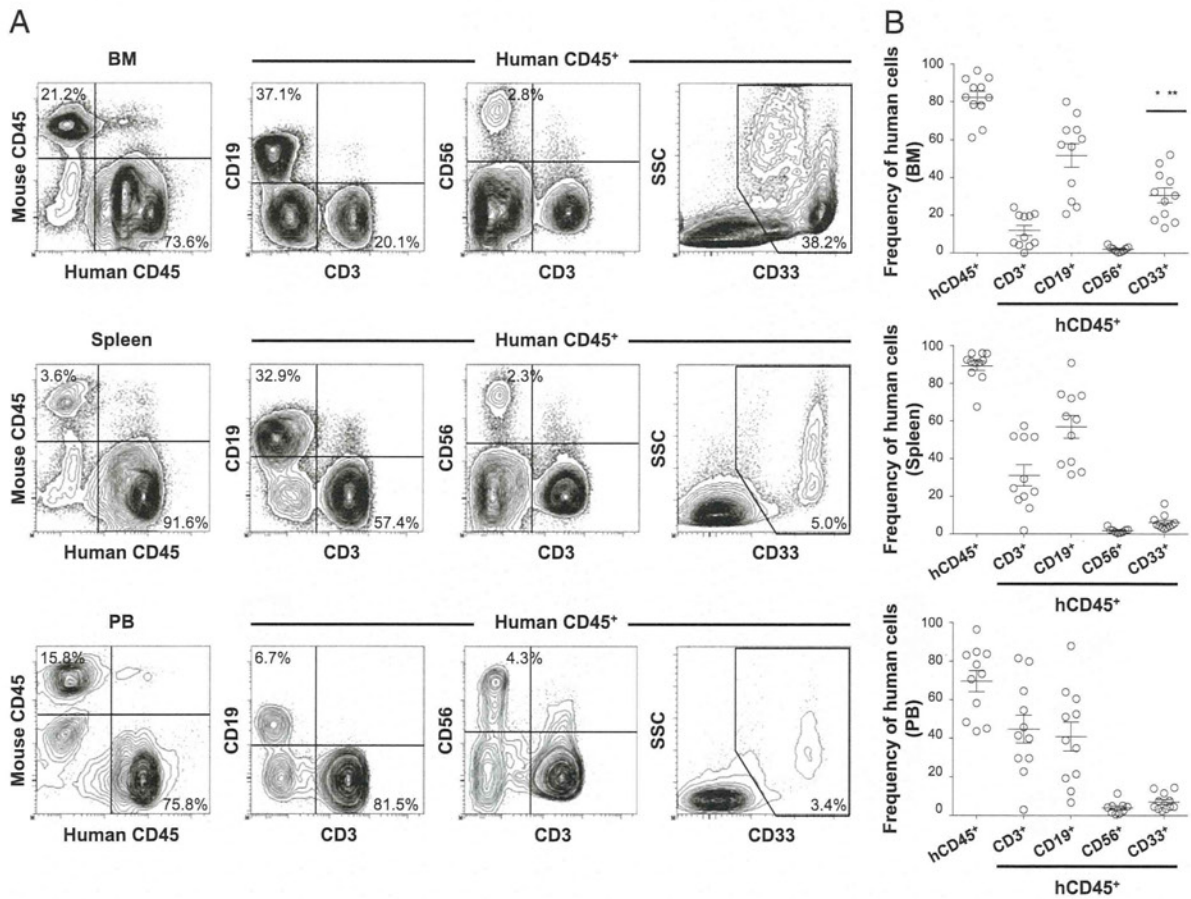

FIGURE 1. Development of human acquired and innate immunity in NSG recipients after transplantation of human CB HSCs. (**A**) Representative sets of flow cytometry contour plots demonstrating the development of human $CD45^+$ hematopoietic cells, $hCD3^+$ T cells, $hCD19^+$ B cells, $hCD56^+$ NK cells, and $hCD33^+$ myeloid cells in the BM, spleen, and PB of an NSG recipient. (**B**) Human $CD45^+$ hematopoietic chimerism and the frequencies of $hCD3^+$ T, $hCD19^+$ B, $hCD33^+$ myeloid cells ($n = 11$ each, frequency of myeloid cells in BM compared with spleen, $*p < 0.0001$, and with PB, $**p < 0.0003$) and $hCD56^+$ NK ($n = 9$ each) cells in the BM, spleen, and PB of NSG recipients at 4–6 mo posttransplantation are summarized.

of NSG recipients at 4–6 mo posttransplantation, we observed differentiation of both human granulocytes and APCs. Among the granulocyte lineage, human $CD15^+CD33^{low}HLA\text{-}DR^-$ neutrophils, $CD117^-CD123^+CD203c^+$ basophils, and $CD117^+CD203c^+HLA\text{-}DR^-$ mast cells were observed in the recipient BM and spleen. Analyses of APC populations found that $CD14^+CD33^+HLA\text{-}DR^+$

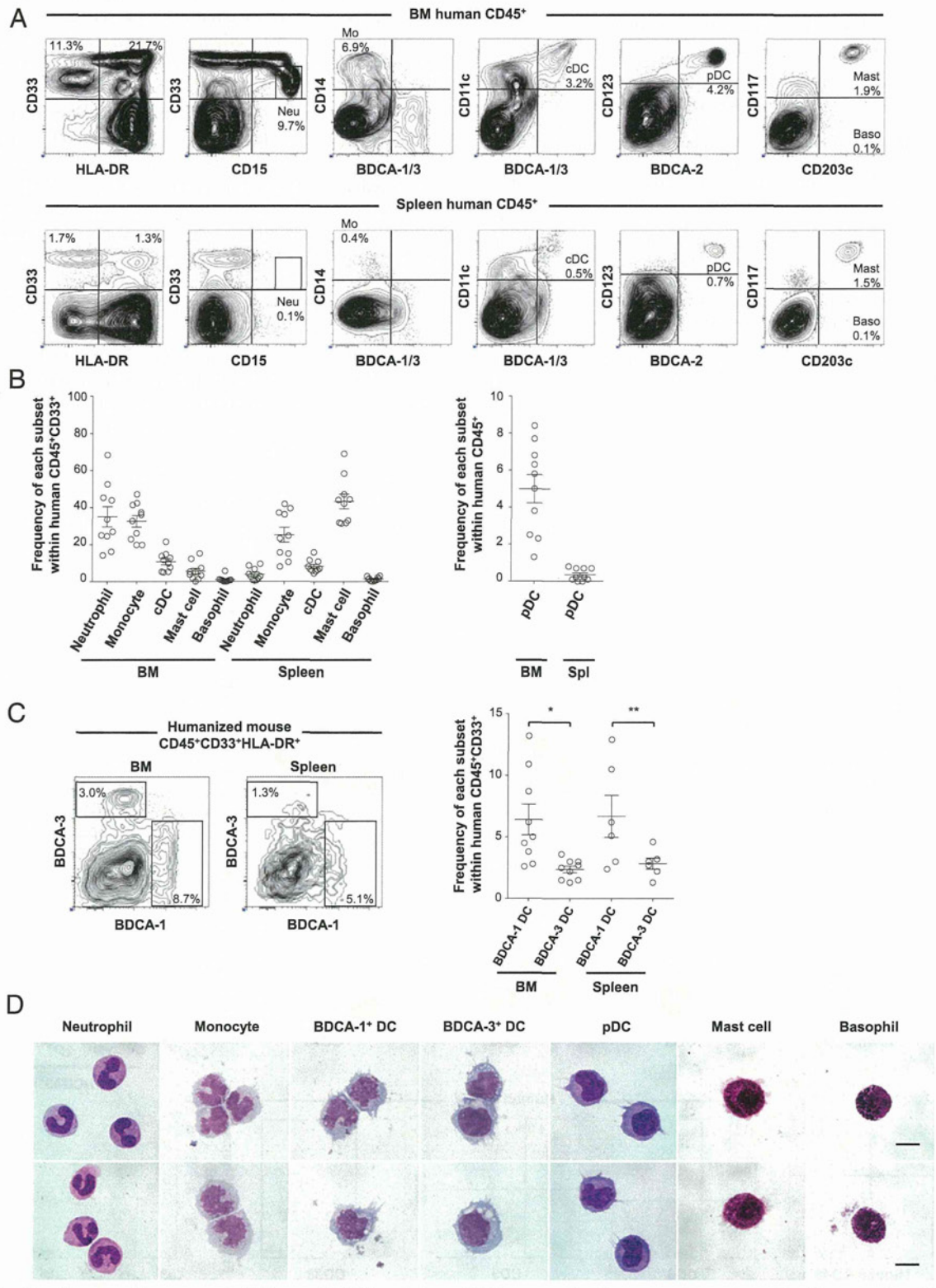

FIGURE 2. Development of human myeloid lineages in NSG recipients. (**A**) Representative flow cytometry contour plots demonstrating differentiation of human $HLA\text{-}DR^-$ granulocytes and $HLA\text{-}DR^+$ APCs in the BM and spleen of an NSG recipient. (**B**) The frequencies of human neutrophils, monocytes, cDCs, mast cells, basophils, and pDCs in the BM and spleen of NSG recipients are summarized ($n = 10$). (**C**) In the humanized mouse BM and spleen, two distinct subsets of DCs, $BDCA\text{-}1^+$ DCs and $BDCA\text{-}3^+$ DCs, were identified in $HLA\text{-}DR^+CD33^+CD11c^+$ conventional DCs. Frequencies of the two DC subsets within BM and spleen $hCD45^+CD33^+$ cells are shown (BM, $n = 9$, $^*p = 0.007$, significant differences between cDCs; spleen, $n = 6$, $^{**}p = 0.046$). (**D**) Human myeloid cells isolated by cell sorting of recipient BM demonstrate characteristic morphological features on May–Grünwald–Giemsa stain. Baso, Basophils; Mast, mast cells; Mo, monocytes; Neu, neutrophils. Scale bars, 10 μm.

BDCA-1$^-$BDCA-3$^-$ monocytes, CD14$^-$CD33$^+$HLA-DR$^+$BDCA-1$^+$ or BDCA-3$^+$ cDCs, and CD123$^+$BDCA-2$^+$HLA-DR$^+$ pDCs developed in the recipients BM and spleen (Fig. 2A, 2B). The frequency of CD15$^+$CD33^{low}HLA-DR$^-$ neutrophils within human CD45$^+$CD33$^+$ myeloid cells were present at the highest level in the BM (35.0 ± 5.4%, n = 10), whereas CD117$^+$CD203c$^+$FcεRI^{low} HLA-DR$^-$ mast cells developed at a higher efficiency in the recipient spleen (43.3 ± 4.0% within CD45$^+$CD33$^+$, n = 10) (Fig. 2B). Among human APCs developing in the NSG recipients, monocytes accounted for the highest frequency in total myeloid cells both in the BM (32.6 ± 3.1%, n = 10) and spleen (25.2 ± 4.0%, n = 10). cDCs are divided into two subsets according to the expression of BDCA-1 and BDCA-3. Within human CD45$^+$CD33$^+$ myeloid cells, the frequencies of BDCA-1$^+$ DCs accounted for 6.4 ± 1.2% in BM (n = 9) and 6.7 ± 1.7% in spleen (n = 6) and were significantly higher than those of BDCA-3$^+$ DCs (2.4 ± 0.3% and 2.8 ± 0.4%, respectively) (Fig. 2C). We then performed flow cytometric analysis using the same mAbs to determine the frequencies of each myeloid subset in primary BM MNCs. Although we could not directly compare human neutrophil development, the proportion of human monocytes, BDCA1$^+$ cDCs, BDCA3$^+$ cDCs, and pDCs was similar between primary human BM and humanized mouse BM (Supplemental Fig.1). In addition to the expression analysis of cell surface molecules, we performed May–Grünwald–Giemsa staining to identify the morphology of the myeloid lineage cells developing in the NSG recipients. Human myeloid cells purified from NSG recipient BM exhibited characteristic morphological features (Fig. 2D).

Human myeloid lineage cells developing in NSG recipients demonstrate intact functional responses to human cytokines in vitro and in vivo

We confirmed the development of various human myeloid subsets in the BM and spleen of NSG recipients and next examined the expression of human cytokine receptors including IFN-γR, G-CSFR, GM-CSFR, and M-CSFR compared with that in human CB (Fig. 3A–C). By using human CD45$^+$CD33$^+$ CB myeloid cells as control, we confirmed that human CD45$^+$CD33$^+$ cells in the recipient BM expressed comparable levels of IFN-γR, G-CSFR, GM-CSFR and M-CSFR (n = 5, no significant difference between humanized mouse BM and CB, p = 0.6444, p = 0.0985, p = 0.3879, and p = 0.5816, respectively) (Fig. 3D).

To demonstrate functional responses to human cytokine stimulation at a cellular level, we examined the phosphorylation of STAT molecules using flow cytometry. Recent studies have revealed that hematopoietic cytokine receptor signaling is largely mediated by JAK kinases and STAT molecules known as the downstream transcription factors (18). BM cells from NSG recipients (n = 3) were

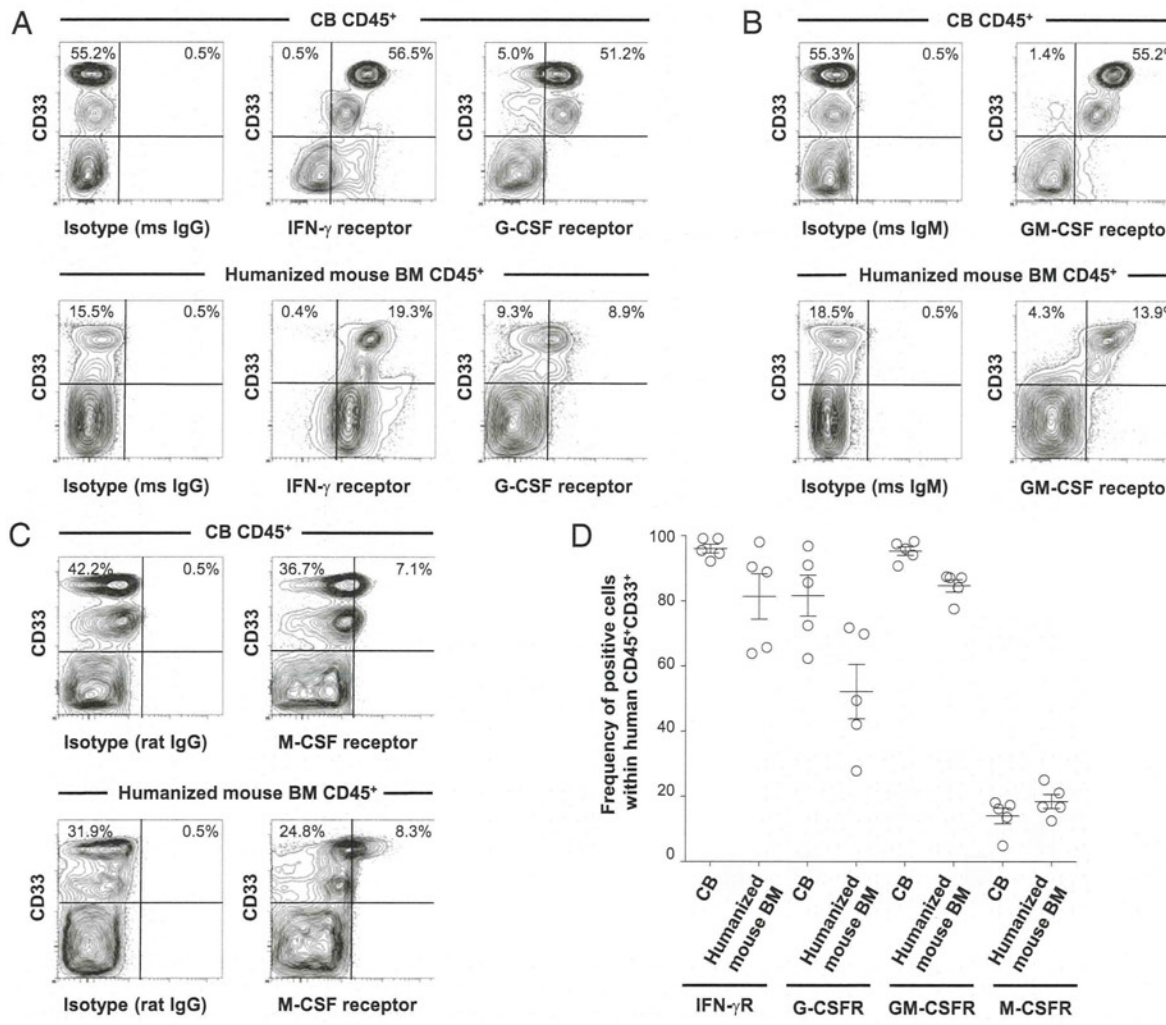

FIGURE 3. Expression of cytokine receptors on human myeloid cells in NSG recipients. (**A**–**C**) Representative flow cytometry contour plots demonstrating the expression of IFN-γR, G-CSFR, GM-CSFR, and M-CSFR by CB hCD45$^+$CD33$^+$ myeloid cells (top) and by hCD45$^+$CD33$^+$ myeloid cells derived from humanized NSG BM (bottom). Contour plots for isotype control Ig are also shown. (**D**) Expression of each cytokine receptor within hCD45$^+$CD33$^+$ cells is summarized (CB, n = 5; humanized NSG BM, n = 5).

stimulated with rhIFN-γ, rhG-CSF, rhGM-CSF, or rhM-CSF in vitro for 15 min at 37°C. In neutrophils and monocytes, rhGM-CSF specifically induced STAT5 phosphorylation, but not irrelevant STATs (e.g., STAT4 and STAT6) (Fig. 4A, 4C). Additionally, rhIFN-γ and rhG-CSF induced optimal STAT phosphorylation (Fig. 4B, 4D, 4E). Indeed, rhIFN-γ stimulation resulted in intracellular STAT1, STAT3, and STAT5 phosphorylation, and rhG-CSF stimulation induced STAT3 and STAT5 phosphorylation, respectively (Fig. 4E). These results indicate that intact molecular events occur in human neutrophils and monocytes in response to recombinant human cytokines in vitro.

We next investigated in vivo cytokine response by human myeloid cells in the NSG humanized mice. Stimulation with rhG-CSF in vivo is known to induce proliferation of myeloid precursors and mobilization of myeloid subsets from BM (19). After in vivo treatment of humanized mice by rhG-CSF for 5 d, the frequencies of $hCD45^+CD15^+CD33^{low}$ fraction (human neutrophils) and $hCD45^+CD15^{-/low}CD33^+$ fraction (human monocytes and DCs) increased in the PB (three out of three recipients) (Fig. 4F). These findings indicate that human myeloid cells developing in the humanized NSG recipients demonstrate functional cytokine response both in vivo and in vitro.

Human inflammatory response via TLR signaling

Along with the role of cytokine receptor signaling in development and function of myeloid cells, signaling via TLRs serves fundamental roles in evoking systemic inflammatory response by myeloid cells (20). We therefore analyzed the expression of TLRs in human myeloid cells developed in the engrafted NSG recipients by flow cytometry. We examined the surface expression of TLR2 and TLR4 in the human myeloid cells developed in the humanized mouse BM. TLR2 is specifically expressed in human monocytes and $BDCA1^+$ DCs, and TLR4 is expressed in the four distinct myeloid subsets, neutrophils, monocytes, $BDCA1^+$ cDCs, and $BDCA3^+$ cDCs (Fig. 5A, 5B). The expression of TLR4 was also confirmed in humanized mouse BM-derived monocytes and other myeloid subsets, which has led us to investigate the in vivo response of human innate immunity against LPS, a potent TLR4

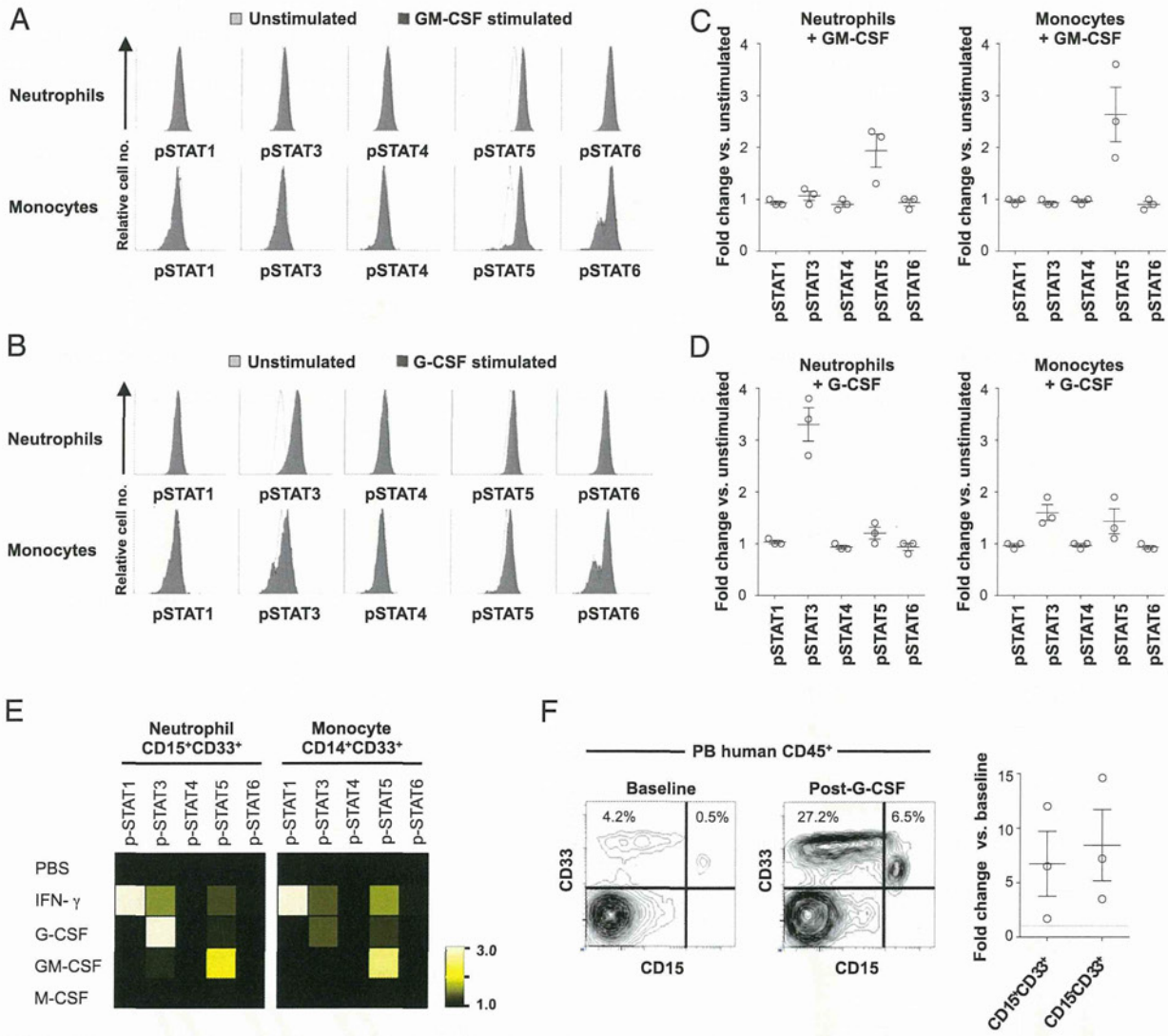

FIGURE 4. Human myeloid lineage cells developing in NSG recipients demonstrate cytokine responses in vitro and in vivo. (**A** and **B**) Phosphorylation of STAT1, STAT3, STAT4, STAT5, and STAT6 in human neutrophils and monocytes derived from an NSG recipient BM after in vitro stimulation with rhGM-CSF (A) and with rhG-CSF (B) was measured by flow cytometry. (**C** and **D**) Results from three independent experiments using three different recipients are summarized. (**E**) Heat map representation of STAT phosphorylation in human neutrophils and monocytes in an NSG recipient BM after in vitro cytokine treatment relative to PBS exposure is shown. (**F**) Representative flow cytometry contour plots demonstrating expansion of myeloid lineage cells in the PB of an NSG recipient in response to in vivo rhG-CSF administration. Frequencies of $hCD45^+CD15^+CD33^{low}$ and $hCD45^+CD15^{-/low}CD33^+$ myeloid cells were increased after in vivo rhG-CSF treatment in PB of NSG recipients for 5 d.

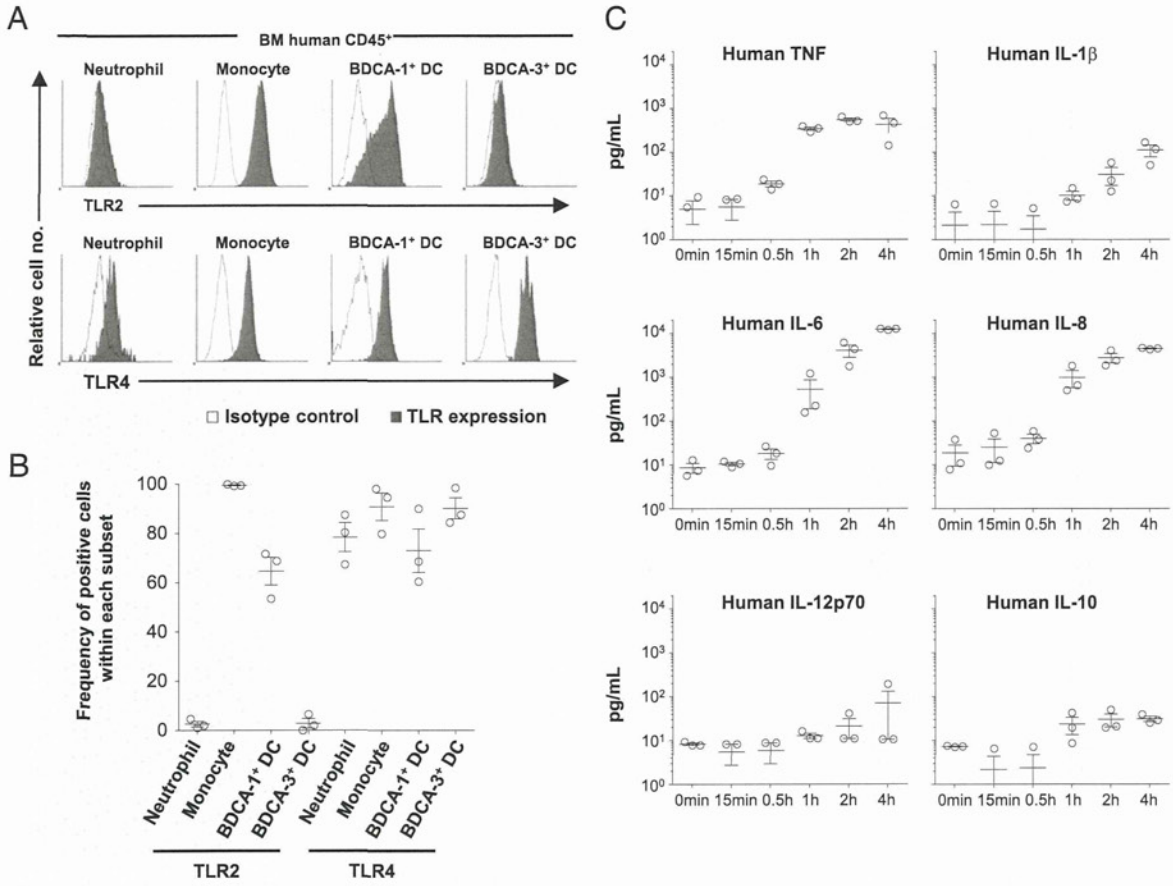

FIGURE 5. Expression of TLRs and response to TLR adjuvant by humanized mouse-derived myeloid subsets. TLR expression is analyzed in the granulocytes, monocytes, and cDCs derived from the humanized NSG recipient BM. (**A** and **B**) Expression of TLR2 and TLR4 in neutrophils, monocytes, BDCA-1$^+$ DCs, and BDCA-3$^+$ DCs was analyzed by flow cytometry. (**C**) At different time points after the injection of 15 μg LPS into humanized NSG recipients, human-specific cytokine levels in plasma were evaluated by cytometric bead array (n = 3).

ligand and endotoxin. To this end, we have administered 15 μg LPS to NSG humanized mice followed by detection of human inflammatory cytokines by flow cytometry. Bead-attached Abs for human cytokines did not detect 5000 pg/ml of mouse cytokines demonstrating that these Abs and analyses are human-specific (Supplemental Fig. 2). Of the cytokines examined, we have seen the significant elevation of plasma levels of human IL-6, human IL-8, and human TNF (Fig. 5C). Time-dependent kinetics showed that the prompt response of human innate cells to the LPS was achieved between 30 min and 1 h after injection. Consequently, humanized mice could be used to examine human innate immune response against infectious organisms and to predict inflammatory response provoked by the TLR ligands.

Human myeloid cells present in NSG recipient lung exhibit functional phagocytosis

In the human immune system, myeloid cells serve an important role in immune surveillance not only in the systemic immune compartments but also in the mucosal tissues, especially the respiratory compartment of lung protected by both mucosal and systemic immune systems (21, 22). To examine whether functional reconstruction of human myeloid cells occurs in the lung, we evaluated the differentiation and function of human myeloid lineage cells isolated from the lungs of NSG recipients. Among human CD45$^+$ cells present in the NSG recipient lung, myeloid lineage cells constituted 20.3 ± 3.8% (n = 8; a representative set of flow cytometry plots shown in Fig. 6A). The majority of human myeloid lineage cells residing in the recipient lungs were CD33$^+$ CD14$^+$HLA-DR$^+$ monocytes/macrophages (60.9 ± 5.1% within huCD45$^+$CD33$^+$, n = 8) (Fig. 6B).

The respiratory tract represents a major port of entry for inhaled pathogenic organisms, and resident alveolar monocytes/macrophages play a major role in surveillance and immune defense. To confirm the phagocytic function of human monocytes/macrophages present in the lungs of NSG recipients, we performed in vitro phagocytosis assay using yellow-green fluorescent beads by flow cytometry and confocal microscopy imaging. After in vitro incubation of NSG recipient-derived human CD45$^+$ cells with 1 and 2 μm fluorescent beads at 37°C, uptake of beads was noted in 9.0 and 7.9% of hCD45$^+$CD33$^+$ human myeloid cells, respectively (Fig. 6C). It should be noted that uptake of fluorescent beads was observed only in hCD45$^+$CD33$^+$ myeloid cells, but not in hCD45$^+$CD33$^-$ lymphoid cells (Fig. 6C). This demonstrates that the fluorescent bead uptake specifically represents phagocytotic function by human lung myeloid cells, not nonspecific uptake of the beads or binding or coating of the cells by the beads. The efficiency of uptake was 24.4 ± 3.0% in the lung-derived hCD45$^+$CD33$^+$ cells (n = 6, p = 0.001 compared with 4°C incubation by two-tailed t test), equivalent to that in BM-derived hCD45$^+$CD33$^+$ cells (16.6 ± 2.7%, n = 4, p = 0.01 compared with 4°C incubation by two-tailed t test) (Fig. 6C, 6D).

Next, phagocytosis of fluorescent beads by human myeloid cells was confirmed by direct visualization by confocal microscopy. Three-dimensional confocal imaging demonstrated intracellular localization of the fluorescent bead signal in sorted fluorescent bead (YG signal)$^+$hCD45$^+$CD33$^+$ human myeloid cells, confirming the

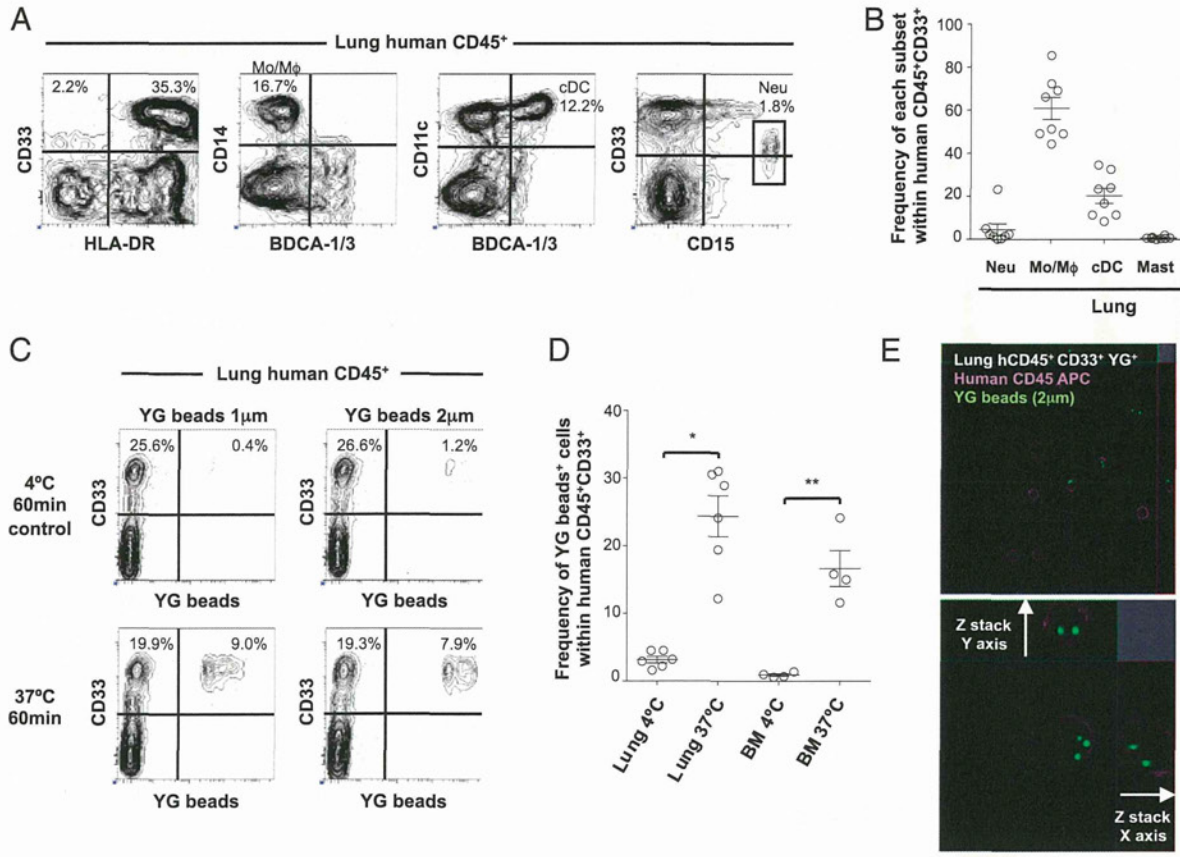

FIGURE 6. Human monocytes/macrophages developing in NSG recipient lung demonstrate phagocytosis of microparticles. (**A**) Representative contour plots demonstrating the reconstitution of human myeloid cells in the lungs of an NSG recipient. Human CD45$^+$ cells within lung cell populations were analyzed by CD33, HLA-DR, CD14, CD11c, BDCA-1/3, and CD15 to identify monocytes/macrophages, cDCs, and neutrophils. (**B**) The frequencies of human neutrophils, monocytes/macrophages, cDCs, mast cells, and basophils within hCD45$^+$CD33$^+$ NSG recipient lung are summarized ($n = 8$). (**C**) A set of representative flow cytometry plots demonstrating the presence of hCD45$^+$CD33$^+$fluorescent beads$^+$ cells. (**D**) Summary of the frequency of hCD45$^+$ CD33$^+$fluorescent bead$^+$ cells in NSG recipient lung cell populations incubated at 37°C and at 4°C (control), respectively, with fluorescent beads (lung, $n = 6$; BM, $n = 4$; $*p = 0.001$, $**p = 0.01$). (**E**) Confocal imaging of FACS-purified hCD45$^+$CD33$^+$fluorescent beads$^+$ cells derived from NSG recipient lung cell populations show internalization of fluorescent beads (green) within hCD45 (purple)-expressing human myeloid cells. Baso, Basophils; Mast, mast cells; Mo/Mϕ, monocytes/macrophages; Neu, neutrophils.

internalization of microparticles by human monocytes/macrophages (Fig. 6E). Taken together, these findings demonstrate the presence of human innate immunity with intact phagocytic function in the NSG recipient lung.

Humanized mouse BM-derived monocytes/macrophages exhibit IFN-γ–induced phagocytosis and killing against Salmonella typhimurium

Myeloid subsets serve essential roles in host defense against various infectious microorganisms as a part of innate immunity. Of the various myeloid subsets discussed in the current study, monocytes and macrophages display excellent phagocytic potential by phagolysosome formation, by the effects of oxidative and nitrosative stress, and by antimicrobial cationic peptides and enzymes (23). To evaluate future application of the humanized mouse system in infectious disease research, we examined the phagocytic function of human monocytes/macrophages derived from humanized NSG BM against *S. typhimurium*. We purified mCD45$^-$TER119$^-$hCD45$^+$ Lin$^-$CD11b$^+$ cells as monocytes/macrophages from the recipient BM (Fig. 7A) and cultured 10,000 purified human monocytes/macrophages with *S. typhimurium* at an MOI of 20 with or without prestimulation of human recombinant IFN-γ at 1000 U/ml. In the five in vitro experiments, stimulation of human monocytes/macrophages with rhIFN-γ resulted in the significantly potentiated phagocytosis and killing of *Salmonella* by the humanized mouse-derived monocytes/macrophages as evidenced by the decreased numbers of colony formation by *S. typhimurium* (at 3 h postinfection $p = 0.023$, at 12 h postinfection $p = 0.091$ [n.s.] compared with control versus IFN-γ stimulation by two-tailed t test) (Fig. 7B). Taken together, human monocytes that develop in the humanized NSG mice possess phagocytic activity against microbeads and bacteria and kill phagocytized bacteria presumably via signaling through cytokine receptors and TLRs.

Discussion

In vivo reconstitution of mature and functional human myeloid cells not only facilitates in vivo examination of human innate immunity but also offers a promising platform for translational research in the areas of infectious immunity and drug development. In the current study, we have aimed to clarify how functional human myeloid cells develop in NSG humanized mice.

In the NSG recipients, we found distinct levels of reconstitution of myeloid subsets in the BM and spleen. The differential myeloid reconstitution in the humanized hematopoietic organs is comparable to that seen in the human tissues, reflecting the distinct physiological roles of each hematopoietic organ in mammals. BM acts an essential reservoir of short-lived neutrophils and monocytes that readily migrate into sites of infection and inflammation. In addition, BM neutrophils function as paracrine regulators for mobi-

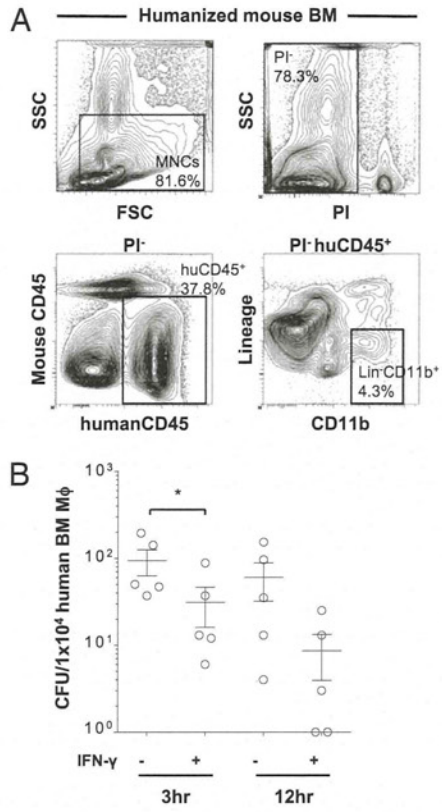

FIGURE 7. Cytotoxicity against *S. typhimurium* by IFN-γ–activated human monocytes/macrophages developing in NSG recipient. (**A**) Within mononuclear cell gate, propidium iodide$^-$ viable, hCD45$^+$Lin$^-$CD11b$^+$ cells were purified from the BM of humanized NSG recipients. Purified BM monocytes/macrophages were stimulated with or without supplementation of 1000 U/ml human IFN-γ for 24 h and then infected with *S. typhimurium* at MOI 20. (**B**) Intracellular CFU was counted at 3 and 12 h postinfection ($n = 5$, $*p = 0.023$ compared with nonstimulated).

lization of HSCs via proteases, such as matrix metalloproteinase-9 (MMP9 or gelatinase B), cathepsin G, and neutrophil elastase contained within intracellular granules. The spleen, a major secondary lymphoid organ, is not only the site of B cell maturation and APC interactions with T and B cells but also is an organ supporting the development of mast cells from their progenitors (24, 25). Cross-reactivity of murine stem cell factor with human c-Kit$^+$ cells may explain the high frequency of human mast cells observed in the recipient spleen (26).

The development of human myeloid lineages is regulated by various cytokine signals (18, 27). In the current study, we directly compared the frequencies of human myeloid subsets using humanized mouse BM and primary human BM MNCs. As to the development of human APCs, humanized mouse BM recapitulates physiological development of human monocytes and two different subtypes of cDCs. However, we could not directly compare the frequencies of human neutrophils between humanized mouse BM and primary human BM, as we have used frozen BM MNCs. According to the previous reports, the frequency of human neutrophils in the humanized mouse BM is lower than that in the primary human BM (28, 29).

Human myelopoiesis within the mouse microenvironment may occur through multiple cooperative mechanisms. First, mouse cytokines such as stem cell factor, FLT3 ligand, G-CSF, and thrombopoietin may directly stimulate human myelopoiesis by cross-reacting with their respective receptors on human hematopoietic stem and/or myeloid progenitor cells. These human myeloid cells in turn produce cytokines such as GM-CSF and IL-3, resulting in the differentiation, maturation, and maintenance of human granulocytes, monocytes, and DCs. At the same time, the cytokine milieu within the NSG recipient repopulated with human hematopoietic cells may not be completely sufficient, to support human hematopoiesis as evidenced by the relative paucity of human neutrophils in the recipient BM, spleen, and circulation that might suggest the requirement of human cytokine or adhesion molecules in the hematopoietic tissues of the recipients. Recent studies suggested that the induced expression of human cytokines in the mouse environment may lead to enhanced differentiation and maturation of human myeloid subsets including neutrophils (30–33). In the current study, however, human monocytes develop in NSG recipients despite the fact that M-CSF is exclusively produced in non-hematopoietic cells and that murine M-CSF does not cross-react with human M-CSFR. This may be attributable to the redundancy among cytokines such as M-CSF, GM-CSF, and IL-3 as demonstrated in previous studies using M-CSF–deficient mice (34).

As a measure of human myeloid cell function, we investigated cytokine responses in human neutrophils and monocytes developing in the NSG recipients. Consistent with the expression of cytokine receptors identified on the human myeloid cells, neutrophils and monocytes showed intact responses to human cytokines both in vivo and in vitro. Phosphorylation of STAT molecules represents a molecular event downstream of cytokine receptor activation. STAT1 is a key mediator of IFN-γ activation of cells and an indispensable component of IFN-γ–dependent innate defense mechanisms against infections (35). The STAT3 signaling pathway is essential for G-CSF–mediated granulopoiesis (36). Specific phosphorylation of STAT5 may be an essential molecular event enabling generation of granulocytes from myeloid progenitors and proliferation and survival of mature neutrophils (37). STAT4 and STAT6 are essential for mediating IL-12 and IL-4 signaling in Th cells (38, 39). Human myeloid cells developing in humanized NSG recipients responded to human cytokines in a specific manner, as determined by the selective activation of JAK–STAT signaling pathways to corresponding cytokines.

Similar to the analysis of the expression of cytokine receptors and signaling, we showed that human myeloid subsets developing in the NSG humanized mice expressed various TLRs at the protein level. In the analysis of TLR expression in humanized mouse BM-derived cells, specific expression of TLR2 was observed in human monocytes and BDCA1$^+$ cDCs rather than neutrophils or BDCA3$^+$ cDCs. Consistent with the expression of TLR4 in human myeloid subsets, in vivo administration of LPS provoked a potent human inflammatory response as demonstrated by the prompt elevation of plasma hIL-6, hIL-8, and hTNF levels. In addition to the examination of cytokine and TLR signaling in human myeloid cells, we investigated the function of human myeloid cells against bacteria to elucidate whether the humanized mouse system can be applied to the research for infectious immunity. As an example of bacterial infection, we chose *S. typhimurium*, a Gram-negative bacillus causing gastrointestinal infections and invasive diseases, especially in children and immunosuppressed patients (40). IFN-γ mediates signaling to activate monocytes and macrophages in phagocytosis (41, 42). In the analysis of colony formation by *S. typhimurium*, IFN-γ potentiated the phagocytosis and antimicrobial activities of humanized mouse BM-derived monocytes/macrophages against this microorganism.

We observed not only systemic reconstitution of human myeloid subsets but also development of respiratory mucosal immunity in NSG humanized mice. Recent mouse studies revealed the crucial and specific roles of mucosal immunity in immune surveillance and

immunological homeostasis in the respiratory tracts (21, 22). In the recipient lung, unlike the BM or spleen, $CD33^+CD14^+HLA\text{-}DR^+$ macrophages were the predominant myeloid population. Frequencies of human B cells, T cells, and myeloid cells in the recipient lung were distinct from those in the recipient PB, excluding the possibility that the human myeloid cells isolated from the recipient lung are contaminating PB myeloid cells. Importantly, macrophages, the predominant human myeloid subset in the recipient lung, demonstrated intact phagocytic function. Macrophages in the NSG recipients will be compared with the recently reported hGM-CSF and hIL-3 knock-in Rag2KO/IL2rγKO humanized mice showing abundant human macrophages in bronchoalveolar lavage (32). Establishment of an in vivo model of human pulmonary mucosal immunity may enable investigation of in vivo immune surveillance in the respiratory tract and in allergic pulmonary disorders and may allow evaluation of vaccines at preclinical stages (43, 44).

In this study, the reconstitution of both systemic and mucosal human innate immunity was observed in the NSG humanized mice. We performed phenotypic characterization and functional evaluation of human myeloid cells developing in the recipients, including granulocytes and APCs. Humanized mice reconstituted with both lymphoid and myeloid human lineages would facilitate in vivo investigation of interactions between the lymphoid and the myeloid compartments, allowing the dissection of the coordinated human immune response at the level of the whole organism.

Disclosures

The authors have no financial conflicts of interest.

References

1. Mosier, D. E., R. J. Gulizia, S. M. Baird, and D. B. Wilson. 1988. Transfer of a functional human immune system to mice with severe combined immunodeficiency. *Nature* 335: 256–259.
2. McCune, J. M., R. Namikawa, H. Kaneshima, L. D. Shultz, M. Lieberman, and I. L. Weissman. 1988. The SCID-hu mouse: murine model for the analysis of human hematolymphoid differentiation and function. *Science* 241: 1632–1639.
3. Greiner, D. L., R. A. Hesselton, and L. D. Shultz. 1998. SCID mouse models of human stem cell engraftment. *Stem Cells* 16: 166–177.
4. Shultz, L. D., P. A. Schweitzer, S. W. Christianson, B. Gott, I. B. Schweitzer, B. Tennent, S. McKenna, L. Mobraaten, T. V. Rajan, D. L. Greiner, et al. 1995. Multiple defects in innate and adaptive immunologic function in NOD/LtSz-scid mice. *J. Immunol.* 154: 180–191.
5. Takenaka, K., T. K. Prasolava, J. C. Wang, S. M. Mortin-Toth, S. Khalouei, O. I. Gan, J. E. Dick, and J. S. Danska. 2007. Polymorphism in Sirpa modulates engraftment of human hematopoietic stem cells. *Nat. Immunol.* 8: 1313–1323.
6. Oldenborg, P. A., A. Zheleznyak, Y. F. Fang, C. F. Lagenaur, H. D. Gresham, and F. P. Lindberg. 2000. Role of CD47 as a marker of self on red blood cells. *Science* 288: 2051–2054.
7. Hiramatsu, H., R. Nishikomori, T. Heike, M. Ito, K. Kobayashi, K. Katamura, and T. Nakahata. 2003. Complete reconstitution of human lymphocytes from cord blood CD34+ cells using the NOD/SCID/gammacnull mice model. *Blood* 102: 873–880.
8. Ito, M., H. Hiramatsu, K. Kobayashi, K. Suzue, M. Kawahata, K. Hioki, Y. Ueyama, Y. Koyanagi, K. Sugamura, K. Tsuji, et al. 2002. NOD/SCID/gamma (c)(null) mouse: an excellent recipient mouse model for engraftment of human cells. *Blood* 100: 3175–3182.
9. Ishikawa, F., M. Yasukawa, B. Lyons, S. Yoshida, T. Miyamoto, G. Yoshimoto, T. Watanabe, K. Akashi, L. D. Shultz, and M. Harada. 2005. Development of functional human blood and immune systems in NOD/SCID/IL2 receptor gamma chain(null) mice. *Blood* 106: 1565–1573.
10. Shultz, L. D., B. L. Lyons, L. M. Burzenski, B. Gott, X. Chen, S. Chaleff, M. Kotb, S. D. Gillies, M. King, J. Mangada, et al. 2005. Human lymphoid and myeloid cell development in NOD/LtSz-scid IL2R gamma null mice engrafted with mobilized human hemopoietic stem cells. *J. Immunol.* 174: 6477–6489.
11. Traggiai, E., L. Chicha, L. Mazzucchelli, L. Bronz, J. C. Piffaretti, A. Lanzavecchia, and M. G. Manz. 2004. Development of a human adaptive immune system in cord blood cell-transplanted mice. *Science* 304: 104–107.
12. Legrand, N., K. Weijer, and H. Spits. 2006. Experimental models to study development and function of the human immune system in vivo. *J. Immunol.* 176: 2053–2058.
13. McDermott, S. P., K. Eppert, E. R. Lechman, M. Doedens, and J. E. Dick. 2010. Comparison of human cord blood engraftment between immunocompromised mouse strains. *Blood* 116: 193–200.
14. Ishikawa, F., A. G. Livingston, J. R. Wingard, S. Nishikawa, and M. Ogawa. 2002. An assay for long-term engrafting human hematopoietic cells based on newborn NOD/SCID/beta2-microglobulin(null) mice. *Exp. Hematol.* 30: 488–494.
15. Mega, J., J. R. McGhee, and H. Kiyono. 1992. Cytokine- and Ig-producing T cells in mucosal effector tissues: analysis of IL-5- and IFN-gamma-producing T cells, T cell receptor expression, and IgA plasma cells from mouse salivary gland-associated tissues. *J. Immunol.* 148: 2030–2039.
16. Schulz, K. R., E. A. Danna, P. O. Krutzik, and G. P. Nolan. 2007. Single-cell phospho-protein analysis by flow cytometry. *Curr. Protoc. Immunol.* Chapter 8: Unit 8.17.
17. Niedergang, F., J. C. Sirard, C. T. Blanc, and J. P. Kraehenbuhl. 2000. Entry and survival of *Salmonella typhimurium* in dendritic cells and presentation of recombinant antigens do not require macrophage-specific virulence factors. *Proc. Natl. Acad. Sci. USA* 97: 14650–14655.
18. Baker, S. J., S. G. Rane, and E. P. Reddy. 2007. Hematopoietic cytokine receptor signaling. *Oncogene* 26: 6724–6737.
19. Semerad, C. L., F. Liu, A. D. Gregory, K. Stumpf, and D. C. Link. 2002. G-CSF is an essential regulator of neutrophil trafficking from the bone marrow to the blood. *Immunity* 17: 413–423.
20. Kawai, T., and S. Akira. 2010. The role of pattern-recognition receptors in innate immunity: update on Toll-like receptors. *Nat. Immunol.* 11: 373–384.
21. Opitz, B., V. van Laak, J. Eitel, and N. Suttorp. 2010. Innate immune recognition in infectious and noninfectious diseases of the lung. *Am. J. Respir. Crit. Care Med.* 181: 1294–1309.
22. Wissinger, E., J. Goulding, and T. Hussell. 2009. Immune homeostasis in the respiratory tract and its impact on heterologous infection. *Semin. Immunol.* 21: 147–155.
23. Savina, A., and S. Amigorena. 2007. Phagocytosis and antigen presentation in dendritic cells. *Immunol. Rev.* 219: 143–156.
24. Arinobu, Y., H. Iwasaki, M. F. Gurish, S. Mizuno, H. Shigematsu, H. Ozawa, D. G. Tenen, K. F. Austen, and K. Akashi. 2005. Developmental checkpoints of the basophil/mast cell lineages in adult murine hematopoiesis. *Proc. Natl. Acad. Sci. USA* 102: 18105–18110.
25. Hallgren, J., and M. F. Gurish. 2007. Pathways of murine mast cell development and trafficking: tracking the roots and routes of the mast cell. *Immunol. Rev.* 217: 8–18.
26. Kambe, N., H. Hiramatsu, M. Shimonaka, H. Fujino, R. Nishikomori, T. Heike, M. Ito, K. Kobayashi, Y. Ueyama, N. Matsuyoshi, et al. 2004. Development of both human connective tissue-type and mucosal-type mast cells in mice from hematopoietic stem cells with identical distribution pattern to human body. *Blood* 103: 860–867.
27. Manz, M. G. 2007. Human-hemato-lymphoid-system mice: opportunities and challenges. *Immunity* 26: 537–541.
28. Brooimans, R. A., J. Kraan, W. van Putten, J. J. Cornelissen, B. Löwenberg, and J. W. Gratama. 2009. Flow cytometric differential of leukocyte populations in normal bone marrow: influence of peripheral blood contamination. *Cytometry B Clin. Cytom.* 76B: 18–26.
29. Björnsson, S., S. Wahlström, E. Norström, I. Bernevi, U. O'Neill, E. Johansson, H. Runström, and P. Simonsson. 2008. Total nucleated cell differential for blood and bone marrow using a single tube in a five-color flow cytometer. *Cytometry B Clin. Cytom.* 74: 91–103.
30. Rathinam, C., W. T. Poueymirou, J. Rojas, A. J. Murphy, D. M. Valenzuela, G. D. Yancopoulos, A. Rongvaux, E. E. Eynon, M. G. Manz, and R. A. Flavell. 2011. Efficient differentiation and function of human macrophages in humanized CSF-1 mice. *Blood* 118: 3119–3128.
31. Rongvaux, A., T. Willinger, H. Takizawa, C. Rathinam, W. Auerbach, A. J. Murphy, D. M. Valenzuela, G. D. Yancopoulos, E. E. Eynon, S. Stevens, et al. 2011. Human thrombopoietin knockin mice efficiently support human hematopoiesis in vivo. *Proc. Natl. Acad. Sci. USA* 108: 2378–2383.
32. Willinger, T., A. Rongvaux, H. Takizawa, G. D. Yancopoulos, D. M. Valenzuela, A. J. Murphy, W. Auerbach, E. E. Eynon, S. Stevens, M. G. Manz, and R. A. Flavell. 2011. Human IL-3/GM-CSF knock-in mice support human alveolar macrophage development and human immune responses in the lung. *Proc. Natl. Acad. Sci. USA* 108: 2390–2395.
33. Takagi, S., Y. Saito, A. Hijikata, S. Tanaka, T. Watanabe, T. Hasegawa, S. Mochizuki, J. Kunisawa, H. Kiyono, H. Koseki, et al. 2012. Membrane-bound human SCF/KL promotes in vivo human hematopoietic engraftment and myeloid differentiation. *Blood* 119: 2768–2777.
34. Umeda, S., K. Takahashi, M. Naito, L. D. Shultz, and K. Takagi. 1996. Neonatal changes of osteoclasts in osteopetrosis (op/op) mice defective in production of functional macrophage colony-stimulating factor (M-CSF) protein and effects of M-CSF on osteoclast development and differentiation. *J. Submicrosc. Cytol. Pathol.* 28: 13–26.
35. Hu, X., and L. B. Ivashkiv. 2009. Cross-regulation of signaling pathways by interferon-gamma: implications for immune responses and autoimmune diseases. *Immunity* 31: 539–550.
36. McLemore, M. L., S. Grewal, F. Liu, A. Archambault, J. Poursine-Laurent, J. Haug, and D. C. Link. 2001. STAT-3 activation is required for normal G-CSF-dependent proliferation and granulocytic differentiation. *Immunity* 14: 193–204.
37. Kimura, A., M. A. Rieger, J. M. Simone, W. Chen, M. C. Wickre, B. M. Zhu, P. S. Hoppe, J. J. O'Shea, T. Schroeder, and L. Hennighausen. 2009. The transcription factors STAT5A/B regulate GM-CSF-mediated granulopoiesis. *Blood* 114: 4721–4728.
38. Elo, L. L., H. Järvenpää, S. Tuomela, S. Raghav, H. Ahlfors, K. Laurila, B. Gupta, R. J. Lund, J. Tahvanainen, R. D. Hawkins, et al. 2010. Genome-wide profiling of interleukin-4 and STAT6 transcription factor regulation of human Th2 cell programming. *Immunity* 32: 852–862.

39. Saraiva, M., J. R. Christensen, M. Veldhoen, T. L. Murphy, K. M. Murphy, and A. O'Garra. 2009. Interleukin-10 production by Th1 cells requires interleukin-12-induced STAT4 transcription factor and ERK MAP kinase activation by high antigen dose. *Immunity* 31: 209–219.
40. Graham, S. M., and M. English. 2009. Non-typhoidal salmonellae: a management challenge for children with community-acquired invasive disease in tropical African countries. *Lancet* 373: 267–269.
41. Liu, J., X. Guan, and X. Ma. 2007. Regulation of IL-27 p28 gene expression in macrophages through MyD88- and interferon-gamma-mediated pathways. *J. Exp. Med.* 204: 141–152.
42. MacNamara, K. C., K. Oduro, O. Martin, D. D. Jones, M. McLaughlin, K. Choi, D. L. Borjesson, and G. M. Winslow. 2011. Infection-induced myelopoiesis during intracellular bacterial infection is critically dependent upon IFN-γ signaling. *J. Immunol.* 186: 1032–1043.
43. Jambo, K. C., E. Sepako, R. S. Heyderman, and S. B. Gordon. 2010. Potential role for mucosally active vaccines against pneumococcal pneumonia. *Trends Microbiol.* 18: 81–89.
44. Legrand, N., A. Ploss, R. Balling, P. D. Becker, C. Borsotti, N. Brezillon, J. Debarry, Y. de Jong, H. Deng, J. P. Di Santo, et al. 2009. Humanized mice for modeling human infectious disease: challenges, progress, and outlook. *Cell Host Microbe* 6: 5–9.

Vaccine 30 (2012) 6338–6339

Contents lists available at SciVerse ScienceDirect

Vaccine

journal homepage: www.elsevier.com/locate/vaccine

Conference report

Summary for Symposium I on the Development of a More Efficacious Influenza Vaccine Held at the 15th Annual Meeting of the Japanese Society for Vaccinology, Tokyo, 2011

ABSTRACT

Influenza HA split vaccine is widely administered to children and adults worldwide. However, its limited efficacy and weak potential to control the next influenza pandemic has recently been emphasized and has raised serious concerns. These circumstances led the Japanese Society for Vaccinology to organize this symposium to discuss the next generation of influenza vaccine which should be more efficacious and much safer. The symposium covered data assessment of the newly developed H5N1 vaccine, adjuvant development for influenza vaccine, the future threat of H5N1 influenza, measures for its control, and the recent development of a mucosal vaccine.

This symposium was convened at the 15th Annual Meeting of the Japanese Society for Vaccinology in Tokyo, Japan, on December 10, 2011. A brief synopsis of how the symposium was planned precedes the introduction of each presentation.

In mid-October 2009, under the heavy burden of a serious pandemic caused by influenza virus A(H1N1)pdm2009, late Dr. Hitoshi Kamiya, Honorary President of the National Mie Hospital and founding member of the Japanese Society for Vaccinology, convoked a group of Japanese researchers with various expertise in infectious diseases, immunology, virology, pediatrics, pathology, and public health in order to assess the data obtained through the research carried out in Japan to develop H5N1 pandemic vaccine. In discussion at the second meeting, Prof. Hiroshi Kiyono, the University of Tokyo, strongly recommended that the new generation of active and leading scientists in the field of Vaccinology develop a research group and apply to the Ministry of Labor, Health and Welfare of Japan for a government-funded research grant for addressing the issue on the development of novel, effective, and safe H5N1 vaccine. After organizing serial brainstorming meetings led by Dr. Kamiya, we successfully established a task force team under the leadership of Prof. Ken J. Ishii, Osaka University, with the goal of developing a more efficacious and safer influenza vaccine. Unfortunately, during these efforts, Dr. Kamiya passed away due to sudden onset of septic shock. As a result our research team was appointed to continue the work initiated by Dr. Kamiya. This symposium was thus dedicated to an honor of Dr. Kamiya, his tremendous contribution to the control of infectious diseases by vaccine in Japan and each speaker presented the outcome of their projects which carry visions and missions of late Dr. Kamiya. Thus, the audiences of the 15th Annual Meeting of the Japanese Society for Vaccinology could enjoy the group meetings with scientific progress recreated before them.

Prof. Tetsuo Nakayama, Kitasato University, presented the first lecture. He discussed why fever appeared in more than 50% of children who received alum-adjuvanted H5N1 whole virion influenza vaccine. Determination of IgG subclass antibodies in three serial specimens obtained from vaccine recipients revealed that IgG1 and IgG4 were developed in patterns similar to those of natural infection with A(H1N1)pdm2009. He also talked about cytokine production pattern observed in lymphocyte culture under stimulation of various influenza vaccine preparations, suggesting that inflammatory cytokines were produced particularly in lymphocytes from younger volunteers stimulated with alum-adjuvanted whole inactivated vaccine formulation.

Prof. Ken J. Ishii began his talk by reviewing our understanding of signal transmission pathways in the innate immune system combined with the mechanism of action of alum adjuvant. Then, he proceeded to explain the potential of nucleic acid adjuvant in relation to the effectiveness of vaccines and ended his lecture by showing the hopeful prospects for clinical application of adjuvants in new concept vaccines in future development.

Dr. Yoshihiro Sakoda, Hokkaido University, talked about the current status and behavior of the highly pathogenic avian influenza viruses (HPAIV), which has spread worldwide. He emphasized that prompt eradication of HPAIVs in poultry is urgently needed in Asian countries where HPAI has not been controlled to prevent the perpetuation of viruses in the lakes, where aquatic birds nest in summer in Siberia.

The last speaker, Dr. Hideki Hasegawa, National Institute of Infectious Diseases, presented data regarding clinical research on intranasal administration of inactivated whole virion seasonal influenza vaccine (H3N2) in humans and showed successful production of neutralizing antibodies mainly composed of IgA in nasal secretions as well as serum neutralizing antibodies. His data surprised a large number of audiences implying that heterosubtypic immunity was elicited in humans even with inactivated whole virion without any adjuvants.

Prof. Tetsuo Nakayama is President of Kitasato Institute for Life Sciences, Tokyo, Japan, Chairman of this Annual Meeting, and also one of our team members. He arranged this symposium. He worked as a general pediatrician in Saiseikai-Central Hospital, Tokyo, for 15 years and moved to the Department of Virology, Kitasato Institute to do basic research in virology and vaccinology. His research interests include pediatric vaccines, measles, mumps, rubella, DTP vaccines, and vaccine safety issues.

0264-410X/$ – see front matter
http://dx.doi.org/10.1016/j.vaccine.2012.07.091

Prof. Ken J. Ishii is Director of Laboratory of Adjuvant Innovation, National Institute of Biomedical Innovation; Laboratory of Vaccine Science, WPI Immunology Frontier Research Center, Osaka University, Osaka, Japan. His research interests include basic to translational researches on influenza vaccines and their adjuvants. He is especially interested in nucleic acids as an endogenous adjuvant for live and killed viral vaccines and additive adjuvant to many other vaccine applications.

Dr. Yoshihiro Sakoda, Associate Professor of Laboratory of Microbiology, Department of Disease Control, Graduate School of Veterinary Medicine, Hokkaido University, Sapporo, Japan. His research interests include prevention and control of important viral diseases of animals and humans, especially pathogenicity of influenza viruses in animals.

Dr. Hideki Hasegawa, Director of the Department of Pathology, National Institute of Infectious Diseases, Tokyo, Japan. His research interests include human retrovirus HTLV-1, human influenza viruses, and mucosal immunity. He is extending his research to the development of intranasal vaccine against influenza to induce mucosal immunity against the viruses.

This symposium was planned and chaired by Drs. Takuji Kumagai and Hiroshi Kiyono. On behalf of the speakers and the rest of JSV members, we would like to express our appreciation and respect to late Dr. Hitoshi Kamiya for his leadership in the field of Vaccinology in Japan.

Takuji Kumagai *
Kohjinkai Health Care, Kumagai Pediatric Clinic, West 6, Momijidai, Atsubetsu-Ku, Sapporo 004-0013, Japan

Hiroshi Kiyono
Division of Mucosal Immunology, Department of Microbiology and Immunology, The Institute of Medical Science, The University of Tokyo, Tokyo 108-8639, Japan

* Corresponding author. Tel.: +81 11 897 1118; fax: +81 11 897 7572.
E-mail address: tkuma@mb.infosnow.ne.jp (T. Kumagai)

17 July 2012
Available online 18 August 2012

THE JOURNAL OF IMMUNOLOGY

The Airway Antigen Sampling System: Respiratory M Cells as an Alternative Gateway for Inhaled Antigens

Dong-Young Kim, Ayuko Sato, Satoshi Fukuyama, Hiroshi Sagara, Takahiro Nagatake, Il Gyu Kong, Kaoru Goda, Tomonori Nochi, Jun Kunisawa, Shintaro Sato, Yoshifumi Yokota, Chul Hee Lee and Hiroshi Kiyono

J Immunol 2011; 186:4253-4262; Prepublished online 28 February 2011;
doi: 10.4049/jimmunol.0903794
http://www.jimmunol.org/content/186/7/4253

The Journal of Immunology is published twice each month by
The American Association of Immunologists, Inc.,
9650 Rockville Pike, Bethesda, MD 20814-3994.

Print ISSN: 0022-1767 Online ISSN: 1550-6606.

The Airway Antigen Sampling System: Respiratory M Cells as an Alternative Gateway for Inhaled Antigens

Dong-Young Kim,*,†,[1] Ayuko Sato,*,[1] Satoshi Fukuyama,*,[1] Hiroshi Sagara,‡ Takahiro Nagatake,*,§ Il Gyu Kong,*,†,§ Kaoru Goda,* Tomonori Nochi,* Jun Kunisawa,*,¶ Shintaro Sato,* Yoshifumi Yokota,‖ Chul Hee Lee,† and Hiroshi Kiyono*,§,¶,#,**

In this study, we demonstrated a new airway Ag sampling site by analyzing tissue sections of the murine nasal passages. We revealed the presence of respiratory M cells, which had the ability to take up OVA and recombinant *Salmonella typhimurium* expressing GFP, in the turbinates covered with single-layer epithelium. These M cells were also capable of taking up respiratory pathogen group A *Streptococcus* after nasal challenge. Inhibitor of DNA binding/differentiation 2 (Id2)-deficient mice, which are deficient in lymphoid tissues, including nasopharynx-associated lymphoid tissue, had a similar frequency of M cell clusters in their nasal epithelia to that of their littermates, $Id2^{+/-}$ mice. The titers of Ag-specific Abs were as high in $Id2^{-/-}$ mice as in $Id2^{+/-}$ mice after nasal immunization with recombinant *Salmonella*-ToxC or group A *Streptococcus*, indicating that respiratory M cells were capable of sampling inhaled bacterial Ag to initiate an Ag-specific immune response. Taken together, these findings suggest that respiratory M cells act as a nasopharynx-associated lymphoid tissue-independent alternative gateway for Ag sampling and subsequent induction of Ag-specific immune responses in the upper respiratory tract. *The Journal of Immunology*, **2011, 186: 4253–4262.**

The initiation of Ag-specific immune responses occurs at special gateways, M cells, which are located in the epithelium overlying MALT follicles such as nasopharynx-associated lymphoid tissue (NALT) and Peyer's patches (1). Peyer's patches contain all of the immunocompetent cells that are required for the generation of an immune response and are the key inductive tissues for the mucosal immune system. Peyer's patches are interconnected with effector tissues (e.g., the lamina propria of the intestine) for the induction of IgA immune responses specific to ingested Ags (2). NALT also contains all of the necessary lymphoid cells, including T cells, B cells, and APCs, for the induction and regulation of inhaled Ag-specific mucosal immune responses (1, 3). This tissue is rich in Th0-type $CD4^+$ T cells, which can become either Th1- or Th2-type cells (4). NALT is also equipped with the molecular and cellular environments for class-switch recombination of μ to α genes for the generation of IgA-committed B cells and the induction of memory B cells (5, 6). It is thus widely accepted that NALT M cells are key players in the uptake of nasally delivered Ags for the subsequent induction of Ag-specific IgA immune responses (1). As a result, NALT is considered a potent target for mucosal vaccines (1).

A recent study identified NALT-like structures of lymphocyte aggregates with follicle formation in the human nasal mucosa, especially in the middle turbinate of children <2 y old (7). Another recent study showed that, postinfection of mice with influenza via the upper respiratory tract, the levels of Ag-specific Ig observed in the serum and in nasal mucosal secretions after surgical removal of NALT were comparable to those in tissue-intact mice (8). Other studies have demonstrated that Ag-specific immune responses are induced in lymphotoxin-$\alpha^{-/-}$ and $CXCL13^{-/-}$ mice, in which the NALT exhibits structural and functional defects (9, 10). Thus, despite the central role of NALT in the generation of Ag-specific Th cells and IgA-committed B cells against inhaled Ags, these tissues do not appear essential for the induction of Ag-specific immune responses, suggesting that additional inductive sites and/or M cells are present in the upper respiratory tract.

The major goal of our study was to search for an NALT-independent M cell-operated gateway by examining and characterizing the entire nasal mucosa. We were able to identify M cells developed in the murine nasal passage epithelium as an alternative and NALT-independent gateway for the sampling of respiratory Ags and the subsequent induction of Ag-specific immune

*Division of Mucosal Immunology, Department of Microbiology and Immunology, Institute of Medical Science, University of Tokyo, Tokyo 108-8639, Japan; †Department of Otorhinolaryngology, Seoul National University College of Medicine, Seoul 110-744, Korea; ‡Medical Proteomics Laboratory, Institute of Medical Science, University of Tokyo, Tokyo 108-8639, Japan; §Graduate School of Medicine and Faculty of Medicine, University of Tokyo, Tokyo 113-0033, Japan; ¶Graduate School of Frontier Sciences, University of Tokyo, Chiba 277-8561, Japan; ‖Department of Molecular Genetics, School of Medicine, University of Fukui, Fukui 910-1193, Japan; #Immunobiology Vaccine Center, University of Alabama at Birmingham, Birmingham, AL 35294; and **Department of Pediatric Dentistry, University of Alabama at Birmingham, Birmingham, AL 35294

[1]D.-Y.K., A.S., and S.F contributed equally to this work.

Received for publication November 25, 2009. Accepted for publication February 2, 2011.

This work was supported by grants-in-aid from the Ministry of Education, Science, Sports, and Culture and the Ministry of Health and Welfare of Japan. Part of the study was also supported by grants from the Joint Research Project under the Korea–Japan Basic Scientific Cooperation Program for FY 2007, Seoul National University Hospital Research Fund 05-2007-004, and the Waksman Foundation. D.-Y.K. was supported by research fellowships from the Japan Society for the Promotion of Science for Foreign Researchers. S.F., T.N., and T.N. were supported by research fellowships from the Japan Society for the Promotion of Science for Young Scientists.

Address correspondence and reprint requests to Dr. Hiroshi Kiyono, Division of Mucosal Immunology, Department of Microbiology and Immunology, Institute of Medical Science, University of Tokyo, 4-6-1 Shirokanedai, Minato-ku, Tokyo 108-8639, Japan. E-mail address: kiyono@ims.u-tokyo.ac.jp

The online version of this article contains supplemental material.

Abbreviations used in this article: DC, dendritic cell; dLN, draining lymph node; GAS, group A *Streptococcus*; GFP-*Salmonella*, GFP-expressing *Salmonella*; Id2, inhibitor of DNA binding/differentiation 2; NALT, nasopharynx-associated lymphoid tissue; *Salmonella*-GFP, *Salmonella typhimurium* expressing GFP; SEM, scanning electron microscopy; TEM, transmission electron microscopy; TT, tetanus toxoid; UEA-1, *Ulex europaeus* agglutinin-1; WGA, wheat germ agglutinin.

www.jimmunol.org/cgi/doi/10.4049/jimmunol.0903794

responses. Characterization of respiratory M cells should accelerate our understanding of the Ag sampling system at work in the upper respiratory tract.

Materials and Methods

Mice

BALB/c mice were purchased from SLC (Shizuoka, Japan). Inhibitor of DNA binding/differentiation 2 $(Id2)^{-/-}$ mice (129/Sv), generated as previously described (11), were maintained together with their littermate $Id2^{+/-}$ mice in a specific pathogen-free environment at the experimental animal facility of the Institute of Medical Science, University of Tokyo. All experiments were carried out according to the guidelines provided by the Animal Care and Use Committees of the University of Tokyo.

M cell staining

For the preparation of nasal cavity samples for confocal microscopy, we decapitated euthanized mice and then, with their heads immobilized, removed the lower jaw together with the tongue. Using the hard palate as a guide, we then used a large scalpel to remove the snout with a transverse cut behind the back molars. After removing the skin and any excess soft tissue, we flushed the external nares with PBS to wash out any blood within the nasal cavity before freezing the nasal passage tissue in Tissue-Tek OCT embedding medium (Miles, Elkhart, IN) in a Tissue-Tek Cryomold. For immunofluorescence staining, we prepared 5-μm–thick frozen sections by using a CryoJane Tape-Transfer System (Instrumedics, St. Louis, MO), allowed the sections to air dry, and then fixed them in acetone at 4°C. We then rehydrated the sections in PBS and incubated them for a further 30 min in Fc blocking solution. For M cell staining, sections were incubated overnight with rhodamine-labeled *Ulex europaeus* agglutinin-1 (UEA-1; Vector Laboratories, Burlingame, CA) at a concentration of 20 μg/ml and FITC-labeled M cell-specific mAb NKM 16-2-4 (12) at 5 μg/ml or FITC-labeled wheat germ agglutinin (WGA; Vector Laboratories, Burlingame, CA) at 10 μg/ml and counterstained with DAPI (Molecular Probes, Eugene, OR) at 0.2 μg/ml in PBS (13).

Electron microscopic analysis of respiratory M cells

For electron microscopic analysis, the nasal cavity sample was prepared and vigorously washed as described above, and then fixed on ice for 1 h in a solution containing 0.5% glutaraldehyde, 4% paraformaldehyde, and 0.1 M sodium phosphate buffer (pH 7.6). After being washed with 4% sucrose in 0.1 M phosphate buffer, the tissues were incubated in an HRP-conjugated UEA-1 solution (20 μg/ml) for 1 h at room temperature. The peroxidase reaction was developed by incubating the tissues for 10 min at room temperature with 0.02% 3,3′-diaminobenzidine tetrahydrochloride in 0.05 M Tris-HCl (pH 8) containing 0.01% H_2O_2. After being washed with the same buffer, the tissues were fixed again with 2.5% glutaraldehyde in 0.1 M phosphate buffer overnight. The nasal passage tissue was decalcified with 2.5% EDTA solution for 5 d. After being washed three times with the same buffer, samples were fixed with 2% osmium tetraoxide on ice for 1 h before being dehydrated with a series of ethanol gradients. For scanning electron microscopy (SEM), dehydrated tissues were freeze-embedded in *t*-butyl alcohol and freeze-dried, then coated with osmium and observed with a Hitachi S-4200 scanning electron microscope (Hitachi, Tokyo, Japan). For transmission electron microscopy (TEM) analysis, the samples were embedded in Epon 812 Resin mixture (TAAB Laboratories Equipment, Berks, U.K.), and ultrathin (70-nm) sections were cut with a Reichert Ultracut N Ultramicrotome (Leica Microsystems, Heidelberg, Germany). Ultrathin sections were stained with 2% uranyl acetate in 70% ethanol for 5 min at room temperature and then in Reynolds lead citrate for 5 min at room temperature. Sections were examined with a Hitachi H-7500 transmission electron microscope (Hitachi, Tokyo, Japan).

Elucidation of M cell numbers

To examine the numbers of respiratory and NALT M cells, mononuclear cells (including M cells, epithelial cells, and lymphocytes) were isolated from the nasal passages and NALT as previously described, with some modifications (4). In brief, the palatine plate containing NALT was removed, and then NALT was dissected out. Nasal passage tissues without NALT were also extracted from the nasal cavity, and mononuclear cells from individual tissues were isolated by gentle teasing using needles through 40-μm nylon mesh. The total numbers of cells isolated from the two preparations were counted. These single-cell preparations were then labeled with PE–UEA-1 (Biogenesis, Poole, England), and the percentages of UEA-1–positive epithelial cells in the nasal passages and NALT were determined with a flow cytometer (FACSCalibur; BD Biosciences, Franklin Lakes, NJ). The numbers of M cells and goblet cells in the nasal passages and NALT were counted by confocal microscopic analysis according to the patterns of staining with UEA-1 and WGA. That is, the frequencies of M cells ($UEA\text{-}1^+WGA^-$) and goblet cells ($UEA\text{-}1^+WGA^+$) were determined by the enumeration of each type in 100 $UEA\text{-}1^+$ cells. The formula used to estimate the number of M cells was: [(total number of mononuclear cells × percentage of $UEA\text{-}1^+$ epithelial cells) × M cells/$UEA\text{-}1^+$ epithelial cells]. The number of respiratory M cells in $Id2^{-/-}$ mice was calculated in the same manner.

Ag uptake in situ

DQ OVA was purchased from Molecular Probes. *Salmonella typhimurium* PhoPc strain transformed with the pKKGFP plasmid was kindly provided by F. Niedergang (14, 15). Group A *Streptococcus* (GAS; *Streptococcus pyogenes* ATCC BAA-1064) was obtained from the American Type Culture Collection (Manassas, VA), and immunofluorescence staining with FITC-conjugated goat anti-*Streptococcus* A Ab (Cortex Biochem, San Leandro, CA) was used to detect GAS uptake. DQ OVA (0.5 mg), GFP-expressing *Salmonella* (GFP-*Salmonella*) (5×10^8 CFU), or GAS (5×10^8 CFU) was intranasally administered and incubated in situ. Thirty minutes after the intranasal administration, the nasal passages were removed as described above and extensively washed with cold PBS with antibiotic solution to remove weakly adherent and/or extracellular DQ OVA or bacteria, as described (13).

The airway fluorescence-labeled Ag-treated nasal passages were processed for confocal microscopy as described above or for FACSCalibur flow cytometric analysis as follows. Mononuclear cells (including M cells, epithelial cells, and lymphocytes) were physically isolated from the nasal passages and NALT as described above, fixed in 4% paraformaldehyde, and labeled with PE–UEA-1 (Biogenesis, Poole, England). The percentage of green fluorescence (BODYPI FL or GFP)/UEA-1 double-positive nasal passage epithelial cells was determined by using an FACSCalibur (BD Biosciences).

To clarify the uptake of the bacteria by M cells, $UEA\text{-}1^+GFP^+$ cells, which were sorted from the nasal passages of mice intranasally infected with GFP-*Salmonella* by using an FACSAria cell sorter (BD Biosciences) were analyzed under three-dimensional confocal microscopy (Leica Microsystems).

To demonstrate the presence of dendritic cells (DCs) in the submucosa of the nasal passages, especially underneath respiratory M cells, after intranasal instillation of GAS, we used FITC- or allophycocyanin-conjugated anti-mouse CD11c (BD Pharmingen, San Jose, CA) Abs for subsequent confocal microscopic analysis.

Immunization

The recombinant *S. typhimurium* BRD 847 strain used in this study was a double *aroA aroD* mutant that expressed the nontoxic, immunogenic 50-kDa ToxC fragment of tetanus toxin from the plasmid pTET*nir*15 under the control of the anaerobically inducible *nirB* promoter (recombinant *Salmonella*-ToxC) (16). As a control, recombinant *Salmonella* that did not express ToxC was used. The recombinant *Salmonella* organisms were resuspended in PBS to a concentration of 2.5×10^{10} CFU/ml. Bacterial suspensions were intranasally administered by pipette (10 μl/mouse) three times at weekly intervals. To eliminate any possible GALT-associated induction of Ag-specific immune responses from the swallowing of bacterial solutions after intranasal immunization, mice were given drinking water containing gentamicin from 1 wk before the immunization to the end of the experiment and were also subjected to intragastric lavage with 500 μl gentamicin solution before and after intranasal immunization. This protocol successfully eliminated the possibility of the intranasally delivered bacteria becoming deposition in the intestine (Supplemental Fig. 1). The titers of tetanus toxoid (TT)-specific serum IgG and mucosal IgA Abs were determined by end-point ELISA, as described previously (17).

To measure GAS-specific immune responses, GAS was suspended in PBS to a concentration of 2×10^{10} CFU/ml. Ten microliters bacterial suspension was intranasally administered once using a pipette. Six weeks after the administration, serum and nasal washes were prepared, and the titers of GAS-specific Ab were measured by ELISA using a previously described protocol (18).

Statistical analysis

Data are expressed as means ± SD, and the difference between groups was assessed by the Mann–Whitney *U* test. The p values <0.05 were considered to be statistically significant.

Results

Respiratory M cells in single-layer epithelium of the nasal passage

The nasal respiratory epithelium of the mouse is composed mainly of pseudostratified ciliated columnar epithelium (19). However, when H&E-stained sections of the whole nasal cavity were examined, a single-layer epithelium was found to cover some regions of the nasal cavity, especially the lateral surfaces of the nasal turbinates (Fig. 1*A–C*). Frozen sections of nasal passages from naive BALB/c mice were prepared and stained with FITC-WGA (green) and rhodamine–UEA-1 (red), and then counterstained with DAPI (blue). Clusters of UEA-1$^+$WGA$^-$ cells that shared M cell characteristics were found exclusively in the single-layer epithelium of the nasal passage covered by ciliated columnar epithelial cells (Fig. 1*D*, 1*E*). Some respiratory M cells were also occasionally found on the transitional area between the single-layer and stratified epithelium. Notably, respiratory M cells also reacted with our previously developed M cell-specific mAb NKM 16-2-4 (12), demonstrating colocalization of the signals of UEA-1 and NKM 16-2-4 (Fig. 1*F*, 1*G*).

Electron microscopic analysis of respiratory M cells

SEM of the respiratory M cells revealed the characteristic features of M cells: a depressed surface with short and irregular microvilli (Fig. 2*A*, 2*B*). TEM analysis revealed that the respiratory M cell was covered by shorter and more irregular microvilli (with definite UEA-1$^+$ signals; Fig. 2*C*, 2*D*) than were found in neighboring ciliated columnar respiratory epithelial cells (Fig. 2*E*). However, no pocket formation (or pocket lymphocytes) was seen in the basal membranes of respiratory M cells, unlike in NALT M cells (Fig. 2*F*, 2*G*). These findings indicated that the newly identified respiratory M cells had most of the unique morphological characteristics of classical M cells.

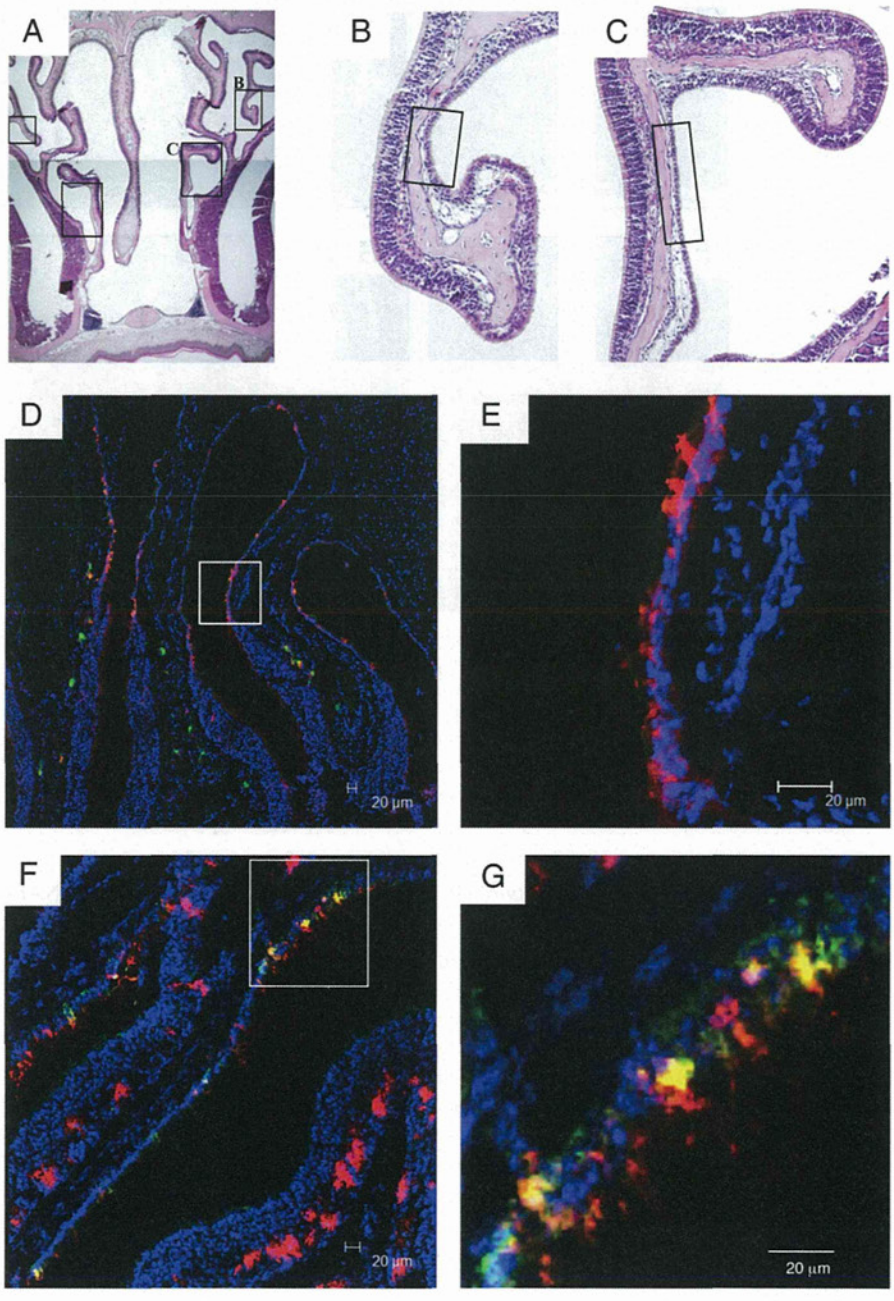

FIGURE 1. Clusters of UEA-1$^+$WGA$^-$ respiratory M cells are found selectively in the single-layer epithelium of the nasal passage. *A–C*, H&E staining reveals the anatomy and general histology of the murine nasal passage (*A*, original magnification ×40). The nasal respiratory epithelium of the mouse is covered with a pseudostratified ciliated columnar epithelium. However, a single-layer epithelium was found on the lateral surfaces of the nasal turbinates (*B*, *C*). Original magnification ×100. Rectangles indicate areas covered with the single-layer epithelium. The results are representative of three independent experiments. *D–G*, Confocal views of UEA-1$^+$ cells in the nasal epithelium of turbinates. Frozen sections were prepared and stained with FITC-WGA (green) and rhodamine–UEA-1 (red), and then counterstained with DAPI (blue) (*D*, *E*). Scale bars, 20 μm. The merged image is shown in *D*. An enlargement of the area in the rectangle in *D* is shown in *E*. UEA-1$^+$WGA$^-$ cells are clustered on the single-layer nasal epithelium of the turbinate. *F* and *G*, UEA-1$^+$ cells also reacted with our previously developed M cell-specific mAb NKM 16-2-4, demonstrating colocalization of signals of rhodamine–UEA-1 (red) and FITC-NKM 16-2-4 (green). The merged image is shown in *F*. An enlargement of an area from the rectangle in *F* is shown in *G*. The results are representative of five independent experiments.

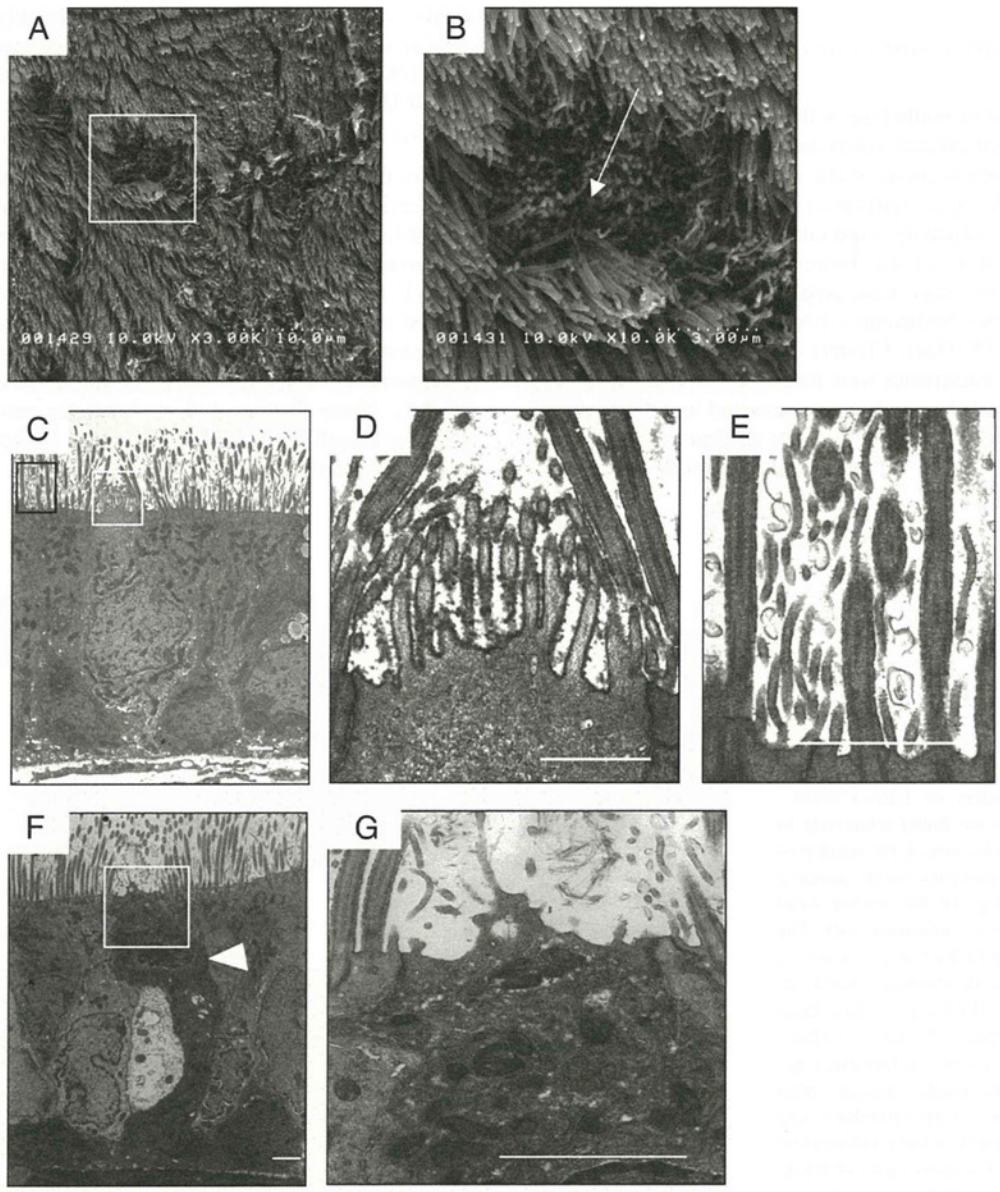

FIGURE 2. Electron microscopic analysis of respiratory M cells. *A* and *B*, SEM analysis shows that the M cells (*B*, arrow) in the nasal passage epithelium are distinguishable from adjacent respiratory epithelial cells by their relatively depressed and dark brush borders. An enlargement of the area in the rectangle in *A* is shown in *B*. As indicated in the *Materials and Methods*, the tissue specimen was incubated with HRP-conjugated UEA-1 before TEM analysis. *C–E*, TEM analysis of respiratory M cells reveals shorter and more irregular microvilli with definite UEA-1$^+$ signals (*D*), unlike the cilia of neighboring respiratory epithelial cells (*E*). *F* and *G*, TEM analysis of NALT M cells. A readily apparent intraepithelial pocket with mononuclear cells (*F*, arrowhead) and short microvilli on the apical surfaces of NALT M cells are seen. The white squares in *C* and *F* indicate UEA-1$^+$ respiratory and NALT M cells, respectively, and are magnified in *D* and *G*, respectively. The black rectangle in *C* indicates an adjacent respiratory epithelial cell and is magnified in *E*. *C–G*, Scale bars, 0.5 μm. Results are representative of four independent experiments.

Protein and bacterial Ag uptake by respiratory M cells

Because M cells were frequently found in the single layer of nasal passage epithelium (Fig. 1*D–G*), we next examined the ability of respiratory M cells to take up various forms of Ag from the lumen of the nasal cavity. DQ OVA or recombinant *Salmonella typhimurium* expressing GFP (*Salmonella*-GFP) was instilled into the nasal cavities of BALB/c mice via the nares. Thirty minutes after the intranasal instillation, immunohistological analyses revealed that the M cells located on the lateral surfaces of the nasal turbinates in the single layer of nasal epithelium had taken up DQ OVA (Fig. 3*A*, 3*B*), as had the M cells located in the NALT epithelium (Fig. 3*C*). Recombinant *Salmonella*-GFP was also observed in M cells in the single layer of nasal epithelium after intranasal administration (Fig. 4*A*, 4*B*). These findings demonstrate that, like NALT M cells (Figs. 3*C*, 4*C*), respiratory M cells were capable of taking up both soluble protein and bacterial Ags.

To further demonstrate the biological significance of respiratory M cells, the numbers of these M cells per mouse were examined and compared with those of NALT M cells (Fig. 3*D*). The number of respiratory M cells was significantly higher than that of NALT M cells. Next, we examined the efficiency of Ag uptake per respiratory M cell and NALT M cell (Figs. 3*E–J*, 4*D–I*). Nasal passage and NALT epithelial cells isolated from BALB/c mice 30 min after intranasal instillation of DQ OVA or recombinant *Salmonella*-GFP were counterstained with PE–UEA-1 for flow cytometric analysis. The UEA-1$^+$ fraction showed a significantly greater efficiency of uptake of DQ OVA Ag and recombinant *Salmonella*-GFP than did UEA-1$^-$ cells isolated from the re-

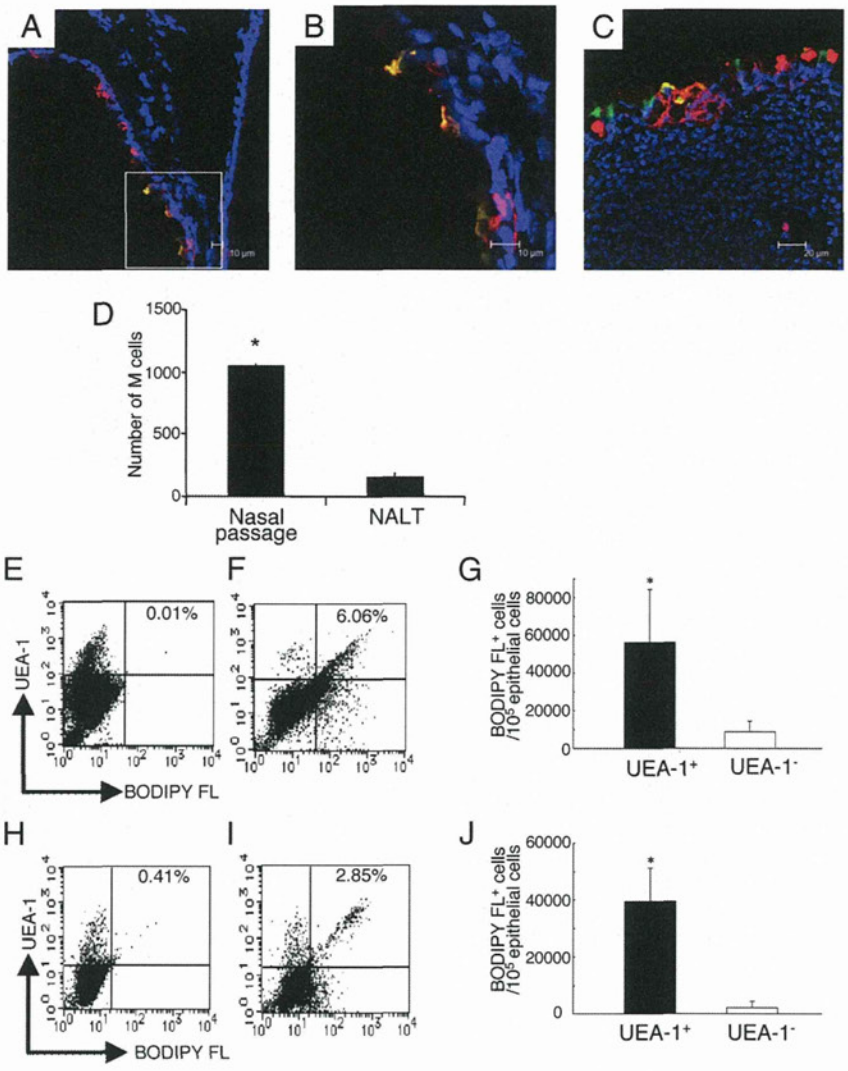

FIGURE 3. Respiratory M cells can take up DQ OVA. *A* and *B*, Immunofluorescence staining of nasal passages in BALB/c mice 30 min after DQ OVA (0.5 mg, green) instillation. Frozen sections of nasal passage were stained with rhodamine–UEA-1 (red) and DAPI (blue). Scale bars, 10 μm. The merged image is shown in *A*. An enlargement of the area in the rectangle in *A* is shown in *B*. These pictures demonstrate DQ OVA uptake by UEA-1$^+$ respiratory M cells. *C*, UEA-1$^+$ (red) NALT M cells in BALB/c mice also show an ability to take up DQ OVA (green). Scale bar, 20 μm. The results are representative of seven independent experiments. *D*, The numbers of UEA-1$^+$WGA$^-$ cells in nasal passages and NALT were quantified. The results are representative of four independent experiments. Flow cytometric analysis of DQ OVA uptake by UEA-1$^+$ respiratory (*E–G*) and NALT (*H–J*) M cells 30 min after intranasal instillation of PBS (*E*, *H*; control) or DQ OVA (*F*, *I*). *G* and *J*, UEA-1$^+$ cells showed significantly higher uptake of DQ OVA than did UEA-1$^-$ cells in the nasal passages and NALT. The results are representative of four independent experiments. $*p < 0.05$.

spiratory epithelium of the nasal passage (Figs. 3*E–G*, 4*D–F*) and NALT (Figs. 3*H–J*, 4*G–I*).

Three-dimensional confocal microscopic analysis demonstrated that UEA-1$^+$ GFP$^+$ cells, which were sorted from the nasal passages of the mice intranasally infected with GFP-*Salmonella*, had captured and taken up the bacteria (Fig. 4*J*, Supplemental Video 1).

Cluster formation by respiratory M cells and DCs in response to inhaled respiratory pathogens

Because respiratory M cells are capable of capturing bacterial Ag, we considered it important to assess these cells as potential new entry sites for respiratory pathogens such as GAS. Confocal microscopic analysis demonstrated that, after its intranasal instillation, GAS stained with FITC–anti-*Streptococcus* A Ab was taken up by UEA-1$^+$ respiratory M cells (Fig. 5*B–E*). SEM analysis also revealed the presence of GAS-like microorganisms on the membranes of respiratory M cells after nasal challenge with GAS (Supplemental Fig. 2*A*). As one might expect, GAS were found in UEA-1$^+$ NALT M cells (Supplemental Fig. 2*B*) as well, confirming a previously reported result (20). Our findings suggest that respiratory M cells act as alternative entry sites for respiratory pathogens.

When we examined the site of invasion by GAS, we noted the presence of CD11c$^+$ DCs underneath the respiratory M cells (Fig. 5). Confocal microscopic analysis of the nasal passage epithelium after intranasal instillation of GAS revealed evidence of the recruitment of DCs, some having contact with the GAS, to the area underneath the respiratory M cells (Fig. 5*B–E*). A few DCs were also observed in the nasal passages of naive mice (Fig. 5*A*); these nasal DCs might preferentially migrate to the area underneath the respiratory M cells to receive Ags from these cells for the initiation of Ag-specific immune responses.

Presence of respiratory M cells in NALT-deficient mice

When we examined the numbers of respiratory M cells in the lymphoid structure-deficient Id2$^{-/-}$ mice (including NALT, NALT-null), the frequency of occurrence of respiratory M cells was comparable to that found in their littermate Id2$^{+/-}$ mice (Fig. 6*A*). This finding suggested that development of respiratory M cells occurred normally under NALT-null or Id2-deficient conditions. Frozen tissue samples were next prepared from NALT-null mice that had received fluorescence-labeled bacteria by intranasal instillation. Immunohistological analysis of these samples revealed the presence of recombinant *Salmonella*-GFP in UEA-1$^+$ cells from the nasal epithelium of Id2$^{-/-}$ mice. GFP-positive bacteria were also located in the subepithelial region of the nasal passages, suggesting that, in the NALT-null mice, some of the nasally deposited bacteria were taken up by respiratory M cells (Fig. 6*B*, 6*C*). Flow cytometric analysis confirmed the uptake of recombinant *Salmonella*-GFP by UEA-1$^+$ M cells, with UEA-1$^+$ cells in the nasal passages of Id2$^{-/-}$ mice showing a significantly higher uptake than UEA-1$^-$ cells (Fig. 6*D–F*).